NASA CONTRACTOR REPORT



NASA CR-2097

# HIGHLY LOADED MULTI-STAGE FAN DRIVE TURBINE - TANDEM BLADE CONFIGURATION DESIGN

*by D. C. Evans and G. W. Wolfmeyer*

*Prepared by*
GENERAL ELECTRIC COMPANY
Cincinnati, Ohio 45215
*for Lewis Research Center*

NATIONAL AERONAUTICS AND SPACE ADMINISTRATION • WASHINGTON, D. C. • AUGUST 1972

| 1. Report No. | 2. Government Accession No. | 3. Recipient's Catalog No. |
|---|---|---|
| NASA CR-2097 | | |

| 4. Title and Subtitle | 5. Report Date |
|---|---|
| HIGHLY LOADED MULTI-STAGE FAN DRIVE TURBINE - TANDEM BLADE CONFIGURATION DESIGN | August 1972 |
| | 6. Performing Organization Code |
| 7. Author(s) | 8. Performing Organization Report No. |
| D. C. Evans and G. W. Wolfmeyer | GE R71 AEG 286 |
| | 10. Work Unit No. |
| 9. Performing Organization Name and Address | |
| General Electric Company<br>Cincinnati, Ohio 45215 | 11. Contract or Grant No.<br>NAS 3-14304 |
| | 13. Type of Report and Period Covered |
| 12. Sponsoring Agency Name and Address | Contractor Report |
| National Aeronautics and Space Administration<br>Washington, D.C. 20546 | 14. Sponsoring Agency Code |

15. Supplementary Notes

Project Manager, Thomas P. Moffitt, Fluid System Components Division, NASA Lewis Research Center, Cleveland, Ohio

16. Abstract

The results of the tandem blade configuration design study are reported. The three stage constant-inside-diameter turbine utilizes tandem blading in the stage two and stage three vanes and in the stage three blades. All other bladerows use plain blades. Blading detailed design is discussed, and design data are summarized. Steady-state stresses and vibratory behavior are discussed, and the results of the mechanical design analysis are presented.

| 17. Key Words (Suggested by Author(s)) | 18. Distribution Statement |
|---|---|
| Turbine, High stage loading, Fan drive turbine, Tandem blading | Unclassified - unlimited |

| 19. Security Classif. (of this report) | 20. Security Classif. (of this page) | 21. No. of Pages | 22. Price* |
|---|---|---|---|
| Unclassified | Unclassified | 66 | $3.00 |

* For sale by the National Technical Information Service, Springfield, Virginia 22151

TABLE OF CONTENTS

## LIST OF TABLES

## LIST OF ILLUSTRATIONS

LIST OF ILLUSTRATIONS (Concluded)

## LIST OF SYMBOLS

| | |
|---|---|
| A | Area ($in.^2$) |
| Aw | Axial width (in.) |
| $C_f$ | Flow Coefficient |
| D | Diameter (in.) |
| $d_i$ | Tandem airfoil passage dimension (in.) |
| $d_o$ | Throat dimension (in.) |
| $\Delta h$ | Turbine energy extraction (Btu/lbm) |
| M | Mach number |
| N | Rotational speed (rev/min) |
| n | Number of vanes or blades |
| $P_S$ | Static pressure (psia) |
| $P_T$ | Total pressure (psia) |
| $T_{HLE}$ | Blade temperature at hub leading edge (°F) |
| $T_S$ | Static temperature (°F) |
| $T_T$ | Total temperature (°F) |
| t | Spacing (in.) |
| $t_e$ | Trailing edge thickness (in.) |
| $t_{max.}$ | Maximum thickness (in.) |
| U | Wheel speed (ft/sec) |
| W | Mass flow rate (lbm/sec) |
| $\alpha_o$ | Vane inlet absolute flow angle (degrees) |
| $\alpha_1$ | Vane exit absolute flow angle (degrees) |
| $\beta_1$ | Blade inlet relative flow angle (degrees) |
| $\beta_2$ | Blade exit relative flow angle (degrees) |

## LIST OF SYMBOLS (Concluded)

| | |
|---|---|
| $\Gamma$ | Stage leaving swirl angle (degrees) |
| $\eta_B$ | Blade efficiency |
| $\eta_{TT}$ | Total-to-Total efficiency |
| $\eta_V$ | Vane efficiency |
| $\sigma$ | Stress (ksi) |
| $\sigma_c$ | Centrifugal stress (ksi) |
| $\sigma_{LE}$ | Stress at blade leading edge (ksi) |
| $\sigma_{TE}$ | Stress at blade trailing edge (ksi) |
| $\sigma_{Hi-c}$ | Stress at maximum distance from axis of least moment of inertia, convex surface (ksi) |
| $\sigma_{Midcv}$ | Stress at maximum distance from axis of least moment of inertia, concave surface (ksi) |
| $\sigma_{lmi}$ | Stress due to bending moment about axis of least moment of inertia (ksi) |
| $\sigma_{mmi}$ | Stress due to bending moment about axis of maximum moment of inertia (ksi) |
| $\Psi_{Zwei}$ | Zweifel number |
| $gJ\Delta h/2U^2$ | Loading factor |

SUBSCRIPTS

| | |
|---|---|
| a | Aft airfoil |
| f | Forward airfoil |

# I. SUMMARY

The results of the detailed design of the tandem blade configuration turbine for Task III of NASA Contract NAS3-14304 are presented. The three-stage constant-inside-diameter turbine utilizes tandem blading in the stage two and stage three vanes and in the stage three blades. All other bladerows use plain blading. The tandem blading philosophy is described. The effects of axial and tangential spacing of the forward tandem airfoils relative to the aft tandem airfoils are discussed. Vane and blade profile design is discussed and detailed blading design data are summarized. Steady state stresses, vibratory behavior and vibratory stability are predicted. The fabrication and testing of a laboratory bench model of the stage three tandem blade is discussed, and the results of the testing are applied to the mechanical design analysis.

## II. INTRODUCTION

The development of high-bypass-ratio turbofan engines for future aircraft propulsion schemes requires the development of fan drive turbines with increasingly higher work output. The requirements of minimized weight and size of such turbofan engines produce a need for turbines with increasingly high stage loading. In order to maintain high turbine efficiencies at high stage loading, advances are required in the technology of producing increased aerodynamic load capability in turbine blading by means of improved design techniques and high-lift devices.

The specific objectives of this program are to:

- Investigate analytically and experimentally aerodynamic means for increasing the turbine stage loading and turbine blade loading consistent with high efficiency for multistage high loaded fan drive turbine configurations.

- Develop sufficient design information to determine the relative importance of changes in engine size, weight, and performance and give primary consideration to use of tandem rotors and stators, where applicable, to reduce weight or extend or improve the blading performance.

- Modify an existing three-stage highly loaded turbine rig and adapt the rig to an overall performance test program of sufficient extent so as to obtain blade element performance.

This is a 24-month analytical and experimental investigation program to provide a turbine high-stage-loading and high-blade-loading aerodynamic technology that will be specifically applicable to multistage fan drive turbine configurations for advanced high-bypass-ratio turbofan propulsion system application. The program will be divided into two phases encompassing nine task items of activity.

The first phase will cover Task Items I, II and III of the program which are to investigate requirements of selected advanced high-bypass-ratio turbofan systems, to carry out parametric turbine vector diagram studies, to conduct a cascade test and evaluation program, to select one design for future study, to complete a detailed aerodynamic turbine design for an existing rig, to complete the detailed blading aerodynamic design for the rig, to perform detailed blading mechanical design for the rig, to perform the turbine rig mechanical design, and to prepare the turbine rig modification drawings required to utilize the existing three-stage highly-loaded-fan turbine rig. The second phase will cover Task Items IV through IX of this program to fabricate, procure, vibration bench test, fatigue endurance test, and inspect the turbine rig modifications; to instrument and calibrate the rig

vehicle; to conduct a test program and to report progress, analysis, and design, as well as test and performance results.

The Task I vector diagram study results have been reported (Reference 1). Based on the results of this study, a velocity diagram was chosen for three highly-loaded turbine configurations: (1) a turbine using plain blades, (2) a turbine using tandem blades and (3) another turbine using high lift devices. The purpose of this report is to present the Task III detailed design of the turbine using tandem blades.

## III. PRELIMINARY DESIGN

### A. REQUIREMENTS

The design requirements for the turbines to be studied were based on engine fan drive turbine requirements. An existing three stage highly loaded fan drive turbine rotating rig was modified for the test and performance phase of this program. Scaling of the turbine to utilize the existing facility was discussed in Reference 2, and the full size and scaled turbine requirements are repeated here.

| Parameter | Full Size | Scaled |
|---|---|---|
| Average Pitch Loading, $\frac{gJ\Delta h}{2\Sigma U_p}2$ | 1.5 | 1.5 |
| Equivalent Specific Work, $E/\Theta_{cr}$, (Btu/lbm) | 33.0 | 33.0 |
| Equivalent Rotative Speed, $N/\sqrt{\Theta_{cr}}$, (rev/min) | 2000 | 3169 |
| Equivalent Weight Flow, $W\sqrt{\Theta_{cr}}\ \varepsilon/\delta$, (lbm/sec) | 70 | 28 |
| Inlet Swirl Angle (degrees) | 0 | 0 |
| Exit Swirl Angle Without Guide Vanes (degrees) | $\leq 5$ | $\leq 5$ |
| Maximum Tip Diameter (inches) | 45.0 | 28.4 |
| Number of Stages | 3 | 3 |
| $W\sqrt{T_T}/P_T$ at Inlet | 108.4 | 43.16 |
| $\Delta h/T_T$ | .0635 | .0635 |
| $N/\sqrt{T_T}$ | 87.7 | 138.98 |

On the basis of these design requirements, a velocity diagram was chosen to be used in the design of all three turbines. The selection of this velocity diagram was discussed in Reference 1, and the final velocity diagram calculation results were presented in Reference 2.

### B. DESIGN PHILOSOPHY

Study of the velocity diagram calculation results indicated that the stage two vane, stage three vane, and stage three blade were the bladerows most likely to benefit from the use of tandem blading. Stage two and stage three vanes have high turning requirements because of the high interstage swirl angles obtained from the velocity diagram calculations, and the stage three blade has a negative reaction hub. Therefore, the tandem

B. DESIGN PHILOSOPHY (Concluded)

blade turbine was comprised of tandem blading in the above mentioned bladerows, and the plain blade hardware described in Reference 2 in all other bladerows.

Studies were conducted to determine the effects of axial and tangential spacing of the forward tandem airfoil sections with respect to the aft tandem airfoil sections. These studies were made using a General Electric potential flow two-cascade computer program. Figures 1 and 2 show typical effects of tangential and axial spacing for a negative reaction rotor section. The amount of surface diffusion is significantly reduced when the leading edge of the aft blade is located near the trailing edge pressure side of the forward blade. After studying these results, the tandem blading was designed by designing the forward and aft airfoil sections to prescribed velocity distributions as individual cascades, followed by the performance of the two-cascade computer analysis of the airfoils in tandem configuration to obtain the final results.

Since it was desired to replace the plain blade hardware with tandem blading in the three bladerows mentioned above, the turbine aerodynamic flowpath was maintained. Thus, the tandem airfoil pairs were designed to the axial widths of the plain blades.

In the design of the tandem airfoils, the same total throat area as had been used in the plain blade design was maintained. Solidities of the forward airfoils were selected using criteria established in Reference 3. Solidities of 1.0 and diffusion factors of 0.5 were selected, and the turning of the forward airfoils was determined. The forward airfoil was treated as a high-turning compressor airfoil, and the remaining design parameters were obtained by using the data presented in Chapter VI of Reference 3. The aft airfoils were designed, using turbine criteria, to do the remaining turning required in each bladerow. The airfoil shapes were designed such that when in the tandem configuration, a converging passage was obtained between the forward airfoil pressure side and the aft airfoil suction side.

In the design of the tandem blading, the objective was to improve the overall velocity distributions relative to the velocity distributions of the plain blading. With the above constraints in mind and a design philosophy established, the detailed aerodynamic design was begun.

## IV. DETAILED AERODYNAMIC DESIGN

### A. SELECTION OF NUMBER OF VANES AND BLADES

Vane and blade solidities were determined through selection of Zweifel numbers based on General Electric design experience using the Zweifel loading criteria. The number of vanes and blades was the same as had been used in the plain blade turbine of Reference 2, with the exception of the stage three stator. Since the vector diagram requirements of the stage two and stage three stator are similar (the inlet and exit angles of the bladerow are similar), little additional knowledge could be expected from testing two very similar tandem stators. By designing and testing a reduced solidity tandem stator in stage three, additional knowledge about the performance of tandem blading could be gained.

A twenty-four percent solidity was chosen for the stage three tandem stator, and analysis showed that a satisfactory velocity distribution around the airfoils could still be obtained. The twenty-four percent reduction in solidity was accomplished by holding $nd_o$ constant (n is the number of vanes, and $d_o$ is the throat dimension as defined in Figure 3). Thus, the total throat area of the stator remained constant. The aerodynamic flowpath showing the number of vanes and blades is presented in Figure 4.

### B. BLADING PROFILE DESIGN

The tandem blading forward and aft airfoils were designed separately using a computer program in which the hub, pitch, and tip section coordinates are developed from a small number of numerical inputs. The axial width of each forward and aft airfoil section was selected on the basis of the knowledge gained in the preliminary design studies. An analysis of flow conditions through each forward and aft section passage was conducted using a potential flow cascade analysis computer program. Design iterations on the forward and aft section profiles were made until satisfactory velocity distributions around each profile were obtained. Forward and aft airfoil sections were paired and the two-cascade computer program was used to determine the velocity distributions around the pairs. Figures 5 through 20 show the final tandem airfoil section flowpaths and the velocity distributions around each tandem pair compared to the velocity distributions around the comparable plain blade sections. In the preliminary design, it was apparent that the stage three rotor plain blade tip had a good velocity distribution, and not much benefit would be obtained from a tandem tip section. Thus, it was decided to design the tip section with the forward and aft airfoils touching in such a manner that when assembled, the tip section in the tandem configuration would nearly conform to the outline of the plain blade tip section. Therefore, no tandem velocity distribution is shown for this section; however, Figure 21 shows the tandem blade tip section compared with the plain blade tip section.

A summary of the tandem vane and blade design data is presented in Tables I through III. The parameters used in the summary are defined in Figure 3.

## C. STACKING

The tandem vane sections were stacked on an axis through the trailing edge of the aft airfoil. The tandem blade hub and tip sections were stacked on an axis through the center of gravity of each tandem pair. The pitch section was positioned such that the passage throat between the forward airfoil pressure side and aft airfoil suction side was linear from hub to tip.

A computer program was employed to generate the coordinates of the sections intermediate to the hub, pitch, and tip. Sections were interpolated at 10%, 30%, 70% and 90% of the aft airfoil trailing edge height for each vane and blade. These coordinates were then used to generate the precision masters required for the fabrication of the vanes and blades. Precision masters for each forward and aft airfoil were generated separately for clarity in fabrication, and reduced copies of these drawings are presented in Figures 22 through 27. Figures 28 through 33 show the stacked forward and aft airfoil sections for each bladerow.

# V. MECHANICAL DESIGN

## A. OVERALL APPROACH

In the initial analysis of the stage three tandem blade, the forward and aft airfoils were treated as though they were separate blades, each mounted on a relatively massive shank, and under a shroud whose proportionate size was based on the individual airfoil tip areas and on the total shroud volume. The initial results of the vibratory behavior and dynamic stability studies indicated a substantial instability of the forward airfoil in its separate blade configuration, and thus a need for a pin or "snubber" between the forward and aft airfoils was established. A pin design was chosen and studies were conducted to determine the behavior of the forward and aft airfoils in the "pinned" tandem configuration.

To provide a means by which a portion of the complex tandem blade behavior might be understood and to provide direction to the overall analytical efforts, a bench model of the tandem blade configuration was constructed, and its behavior was studied.

## B. LABORATORY BENCH MODEL OF TANDEM BLADE

The tandem blade bench model was fabricated from two AISI 403 Stainless Steel low pressure turbine blades which had been designed for a previous air turbine. The model was constructed to be geometrically similar to the actual design. The chord lengths, airfoil twists, tip shroud mass, and the position of the forward airfoil relative to the aft airfoil were essentially correct. Every effort was made to hold other variables such as thickness and camber consistent with the actual tandem blade design values.

The model was used to study the various modes of vibration of the forward and aft airfoils, and of the tandem blade as a system. After testing of the unpinned configuration was completed, a pin was added to join the forward and aft airfoils at the point of maximum vibratory amplitude, and the testing program was repeated. Photographs of the laboratory bench model in the unpinned configuration are shown in Figures 34 and 35.

The importance of the model lies not in the actual numerical results obtained, but rather in the fact that the general vibratory characteristics of the model will be present in the actual design, and that the relative behavior of the pinned to unpinned configurations should also remain constant.

C. VIBRATORY BEHAVIOR

1. Aft Airfoil

The aft airfoil, including its proportionate shroud weight, is substantially more massive than the forward airfoil. Because of this relative massiveness, one set of possible blade frequencies can be obtained by treating the aft airfoil as though it acted independently of the forward airfoil. The frequencies obtained using this approach will differ somewhat from the actual tandem blade frequencies since the forward airfoil adds cross-sectional stiffness over the entire blade length.

From the analytical efforts conducted on the three stage plain blade configuration (Reference 2), it was determined that four sets of boundary conditions could adequately approximate the most probable modes of vibration. These boundary conditions are described as follows:

a. Cantilevered Mode - Cantilevered at the base of the shank, free at the tip shroud. This condition was used to determine the amount of steady-state tip shroud twist or untwist and to obtain lower bounds on certain resonant frequencies.

b. Out-of-Phase Mode - Fixed at the base of the shank, pinned at the tip shroud. The flexure and torsional natural frequencies obtained for these conditions will probably exist under operating conditions.

c. Wheel Mode - Fixed at the base of the shank, restrained at the tip shroud in all directions except axially. Simulates blade behavior in a coupled disc-blade mode. The flexure, axial, and torsional natural frequencies obtained for these conditions will probably exist under operating conditions.

d. Free Slip Mode - Fixed at the base of the shank, adjacent tip shrouds allowed to slip relative to each other. The axial and torsional natural frequencies obtained for these conditions may exist during turbine operation. Steady- state stresses obtained for this set of conditions are probably the most realistic.

The results of the above four conditions were reduced to a set of "Most Probable Frequencies of Vibration" for the aft airfoil and are tabulated below and shown in Figure 36. The most probable frequencies of vibration represent frequencies at the design speed, and small differences resulting from the various boundary conditions have been averaged out.

Most Probable Frequencies of Vibration - Unpinned Aft Airfoil

| Mode of Blade Vibration | Frequency (Hz) | Boundary Conditions Used to Obtain Frequencies |
|---|---|---|
| First axial | 385 | c, d |
| First flexure | 839 | b, c |
| Second flexure | 1646 | b, c |
| First torsional | 2355 | b, c, d |
| Third flexure | 3458 | b, c |
| Second axial | 4598 | c, d |
| Second torsional | 4613 | b, c, d |

2. Forward Airfoil

As was stated above, the aft airfoil is substantially more massive than the forward airfoil. Thus, two general modes of forward airfoil vibration were considered:

a. Forward Airfoil Acting Independently

Because of the large total shank and shroud mass relative to the mass of the forward airfoil, fixed root and fixed tip boundary conditions yield an array of frequencies which are likely to occur during actual turbine operation. The results of the analysis, performed at the design conditions are presented in Figure 37 and tabulated below.

Most Probable Frequencies of Vibration
Unpinned Forward Airfoil Acting Independently

| Mode of Blade Vibration | Frequency (Hz) |
|---|---|
| First flexure | 817 |
| Second flexure | 1440 |
| Third flexure | 2773 |
| First torsional | 3285 |
| First axial | 3570 |
| Approximate frequencies for | 4483 |
| higher modes of | 4542 |
| vibration within range | 4635 |
| of interest | 4749 |
| | 4759 |

Because of the relatively small size of the forward airfoil compared to the aft, it is difficult to expect, at least to a first approximation, any other boundary conditions under which the forward airfoil could act independently of the aft airfoil.

b. Forward Airfoil Driven by Aft Airfoil

Since the aft airfoil is quite large relative to the forward airfoil, it is possible that the forward airfoil will be driven by the aft at the aft airfoil resonant frequencies. This was demonstrated in the testing of the laboratory bench model described above. This behavior gives another array of probable forward blade frequencies which are the same as the aft airfoil frequencies tabulated above.

3. Pinned Airfoil

The rather substantial calculated instability of the forward airfoil in the separate airfoil configuration led to the conclusion that a pin or snubber connecting the forward and aft airfoils near the point of maximum vibratory amplitude was necessary to insure the dynamic stability of the tandem blade under air turbine conditions. The method used to join the two airfoils was a design with "half-pins" which would be machined onto the airfoils during manufacture and welded together at assembly. The pinned configuration is shown in Figure 38.

Many of the conclusions concerning vibratory behavior have been based on results of the unpinned blade analysis in conjunction with laboratory testing of the bench model with the pin added. It was judged that because the pin reduced the effective length of the forward airfoil by about one-half, most of the forward airfoil resonant frequencies will bymoved beyond nozzle passing frequency, and thus out of the region of concern. It is estimated that only three or four frequencies will remain within the region of interest. This substantially reduces the possibility of a resonance problem within the operating range. For the aft airfoil, little deviation from the frequencies listed above is expected due to the large mass and stiffness of the aft airfoil as compared to that of the forward airfoil.

D. VIBRATORY STABILITY

During the early stages of the tandem blade design, it was recognized that the configuration, particularly the forward airfoil, might be dynamically unstable. Analytical efforts were conducted to determine the presence of any instabilities. The stability criteria employed throughout these efforts were based on the "reduced velocity parameters" described below.

$$V_\alpha = \frac{Vr}{(\frac{c}{2})(f_\alpha)} \quad \text{and} \quad V_h = \frac{Vr}{(\frac{c}{2})\ (f_h)}$$

where:

$V_r$ = airfoil inlet or exit (depending upon the configuration) relative gas stream velocity,

c = chord length,

$f_\alpha$ = first torsional frequency,

$f_h$ = first flexure frequency,

and where $V_r$ and c are measured at 50% blade length when fixed root and fixed tip boundary conditions are used, 60% span for the fixed root and shrouded tip boundary conditions, and 87.5% span for fixed root and free tip boundary conditions.

General Electric design experience established the following vibratory stability criteria:

Turbine blades - considered to be dynamically stable for $V_\alpha < 3.0$ and $V_h < 9.0$ when $V_r$ is the exit relative velocity.

Compressor blades - considered to be dynamically stable for $V_\alpha < 1.2$ and $V_h < 3.6$ when $V_r$ is the inlet relative velocity.

These criteria were applied to the tandem configuration turbine analysis.

1. Aft Airfoil

The turbine criteria were applied to the aft airfoil since its shape and position relative to the gas stream are not unlike that of a typical turbine blade. These results were obtained for fixed root-fixed tip boundary conditions:

$$V_\alpha = 1.29 \quad \text{and} \quad V_h = 3.62$$

This indicated a rather substantial margin of vibratory stability. These results were verified by the laboratory testing of the bench model.

2. Forward Airfoil

Since the forward airfoil was treated as a compressor blade during the aerodynamic design, its shape, loading, and position relative to the gas stream are similar to that of a typical compressor blade. Thus, it was decided that the vibratory stability criteria for compressor blades should be applied to the forward airfoil. These results were obtained for fixed root-fixed tip boundary conditions:

$$V_\alpha = 2.04 \quad \text{and} \quad V_h = 5.87$$

This indicated substantial vibratory instability, and a need for a pin or snubber between the airfoils. These results were supported by the vibratory behavior demonstrated by the laboratory model.

3. Pinned Tandem Airfoil

The vibratory frequencies required for the calculation of the reduced velocity parameters were obtained through testing of the laboratory model. The calculated frequencies for the unpinned airfoil were multiplied by the ratio of the experimental pinned airfoil frequencies to the experimental unpinned airfoil frequencies. The reduced velocity parameters for the forward airfoil were then calculated to be:

$$V_\alpha = 1.07 \quad \text{and} \quad V_h = 1.46$$

This indicated that the pinned tandem blade forward airfoil was stable. The aft airfoil stability parameters remained essentially the same as those calculated for the unpinned configuration since the frequencies for the aft airfoil were not significantly altered by the addition of the pin. The tandem blade pinned configuration should be dynamically stable in the air turbine environment.

## E. STEADY-STATE BEHAVIOR

Steady-state mechanical stresses were calculated for the free slip tip shroud boundary conditions for the aft airfoil. The fixed root-fixed tip boundary conditions were used for the forward airfoil. These conditions were believed to be the most realistic for steady-state operation. The stresses were quite low for both the forward and aft airfoils in the unpinned configuration. The results of the analysis are presented in Table IV. Steady-state stresses should be even lower in the pinned configuration. Bending stresses in the region of the pin will increase, but an adequate margin of safety will be maintained. The stress concentration due to the presence of the pin should not be of major concern because of the low stress field in this region.

## F. KEY DETAIL DRAWINGS

The mechanical design flowpath for the air turbine test rig is shown in Figure 39. The detail drawings used for the assembly of the test rig are listed in Table V.

## REFERENCES


1. Evans, D. C.: "Investigation of a Highly Loaded Multistage Fan Drive Turbine, Report for Task I - Vector Diagram Study," NASA CR - 1862, July 1971.

2. Evans, D.C. and Wolfmeyer, G. W.: "Investigation of a Highly Loaded Multistage Fan Drive Turbine - Plain Blade Configuration Design", NASA CR - 1964, November 1971.

3. Lewis Research Center, NASA: "Aerodynamic Design of Axial Flow Compressors, Revised," NASA SP-36, 1965.

TABLE I. STAGE TWO TANDEM VANE DESIGN DATA

| Parameter | Hub | Pitch | Tip |
|---|---|---|---|
| Diameter (trailing edge, in.) | 17.8 | 21.455 | 25.11 |
| $\alpha_o$, (degrees) | 49.4 | 44.4 | 43.4 |
| $\alpha_1$, (degrees) | 61.4 | 58.5 | 58.2 |
| $\Psi$ Zwei, incompressible | .777 | .757 | .730 |
| Aw, (in.) | .91 | 1.175 | 1.44 |
| $Aw_f$, (in.) | .458 | .570 | .676 |
| $Aw_a$, (in.) | .550 | .736 | .920 |
| t, (in.) | .518 | .624 | .730 |
| n | | 108 | |
| $nd_o$ ($C_f$ = .975, $\eta_v$ = .97) | 27.43 | 36.07 | 42.55 |
| $d_o = nd_o/n$, (in.) | .254 | .334 | .394 |
| $t_{e_f}$, (in.) | .020 | .020 | .020 |
| $t_{e_a}$, (in.) | .020 | .020 | .020 |
| $t_{e_a}/(t_{e_a} + d_o)$ | .073 | .057 | .048 |
| Chord $_f$, (in.) | .531 | .632 | .736 |
| Chord $_a$, (in.) | .694 | .910 | 1.136 |
| $t_{max.f}$, (in.) | .056 | .064 | .073 |
| $t_{max.a}$, (in.) | .066 | .076 | .085 |
| $d_i$, (in.) | .052 | .066 | .074 |
| Axial overlap, (in.) | .093 | .119 | .146 |
| Wedge angle $_f$, (degrees) | 7.1 | 6.0 | 8.3 |
| Wedge angle $_a$, (degrees) | 5.1 | 4.8 | 3.5 |
| Unguided turning, (degrees) | 1.8 | 11.9 | 9.8 |
| Overturning, (degrees) | 3.1 | 2.4 | 2.5 |

Precision Master Numbers: Forward Vane: 4012241-962

Aft Vane : 4012241-964

TABLE II. STAGE THREE TANDEM VANE DESIGN DATA

| Parameter | Hub | Pitch | Tip |
|---|---|---|---|
| Diameter (trailing edge, in.) | 17.8 | 22.61 | 27.42 |
| $\alpha_o$, (degrees) | 46.1 | 39.7 | 38.0 |
| $\alpha_1$, (degrees) | 57.0 | 52.2 | 51.7 |
| $\Psi$ Zwei, incompressible | 1.132 | 1.157 | 1.121 |
| Aw, (in.) | 1.0 | 1.3 | 1.6 |
| $Aw_f$, (in.) | .492 | .661 | .829 |
| $Aw_a$, (in.) | .620 | .846 | .987 |
| t, (in.) | .736 | .934 | 1.133 |
| n | | 76 | |
| $nd_o$ ($C_f$ = .975, $\eta_V$ = .97) | 31.2 | 44.5 | 54.6 |
| $d_o = nd_o/n$, (in.) | .410 | .586 | .719 |
| $t_{e_f}$, (in.) | .020 | .020 | .020 |
| $t_{e_a}$, (in.) | .020 | .020 | .020 |
| $t_{e_a} / (t_{e_a} + d_o)$ | .046 | .033 | .027 |
| Chord $_f$, (in.) | .552 | .699 | .856 |
| Chord $_a$, (in.) | .779 | .984 | 1.220 |
| $t_{max._f}$, (in.) | .056 | .074 | .094 |
| $t_{max._a}$, (in.) | .071 | .090 | .110 |
| $d_i$, (in.) | .076 | .086 | .113 |
| Axial overlap, (in.) | .113 | .160 | .213 |
| Wedge angle $_f$, (degrees) | 5.6 | 7.7 | 7.8 |
| Wedge angle $_a$, (degrees) | 7.5 | 6.8 | 6.2 |
| Unguided turning, (degrees) | 18 | 12.8 | 13.0 |
| Overturning, (degrees) | 6.9 | 6.9 | 5.0 |
| Precision Master Numbers | Forward Vane: 4012241-966 | | |
| | Aft Vane : 4012241-968 | | |

TABLE III. STAGE THREE TANDEM BLADE DESIGN DATA

| Parameter | Hub | Pitch | Tip |
|---|---|---|---|
| Diameter (trailing edge, in.) | 17.8 | 23.1 | 28.4 |
| $\beta_1$, (degrees) | 45.5 | 27.1 | 5.6 |
| $\beta_2$, (degrees) | 35.3 | 41.6 | 58.1 |
| $\Psi$ Zwei, incompressible | .937 | 1.001 | .919 |
| Aw, (in.) | 1.22 | 1.05 | .88 |
| $Aw_f$, (in.) | .498 | .438 | .378 |
| $Aw_a$, (in.) | .843 | .730 | .612 |
| t, (in.) | .499 | .648 | .797 |
| n | | 112 | |
| $nd_o$ ($C_f$ = .97, $\eta_B$ = .95) | 46.26 | 55.10 | 47.82 |
| $d_o = nd_o/n$, (in.) | .413 | .492 | .427 |
| $t_{e_f}$, (in.) | .020 | .020 | .020 |
| $t_{e_a}$, (in.) | .020 | .020 | .020 |
| $t_{e_a} / (t_{e_a} + d_o)$ | .046 | .039 | .045 |
| Chord $_f$, (in.) | .572 | .456 | .380 |
| Chord $_a$, (in.) | .848 | .782 | .896 |
| $t_{max._f}$, (in.) | .060 | .057 | .056 |
| $t_{max._a}$, (in.) | .079 | .067 | .055 |
| $d_i$, (in.) | .074 | .038 | 0 |
| Axial overlap, (in.) | .115 | .111 | .098 |
| Wedge angle $_f$, (degrees) | 7.8 | 8.5 | 10.2 |
| Wedge angle $_a$, (degrees) | 8.5 | 6.2 | 2.8 |
| Unguided turning, (degrees) | 9.0 | 8.7 | 10.6 |
| Overturning, (degrees) | -2.4 | 1.6 | 3.4 |
| Precision Master Numbers | Forward Blade: 4012241-970 | | |
| | Aft Blade : 4012241-972 | | |

TABLE IV. STEADY-STATE MECHANICAL STRESSES AND ESTIMATED VIBRATORY CAPABILITIES

Unpinned Separate Airfoil Analysis

| Mechanical Stresses (ksi) | | Forward Airfoil Fixed-Fixed Boundary Condition | Aft Airfoil Free Slip Boundary Condition |
|---|---|---|---|
| Airfoil Hub | | | |
| $\sigma$ centrifugal | | 9.87 | 10.50 |
| $\sigma$ maximum gas bending | | 3.46 (TE) | 38.80 (LE) |
| $\sigma$ resultant span wise stress | LE | 9.64 | 49.30 |
| | TE | 13.33 | 39.13 |
| | Hi-c | 8.36 | -13.95 |
| | Midcv | 10.64 | 14.07 |
| $\sigma$ uncorrected gas bending (lmi and mmi) | LE | 7.52 | 44.33 |
| | TE | 2.50 | 37.94 |
| | Hi-c | 5.56 | -29.66 |
| | Midcv | 2.66 | 4.29 |
| $\sigma$ corrected gas bending (lmi and mmi) | LE | 6.34 | 26.53 |
| | TE | 2.50 | 22.24 |
| | Hi-c | -4.85 | -17.60 |
| | Midcv | 2.33 | 2.55 |
| Under Tip Shroud | | | |
| $\sigma$ centrifugal | | 7.79 | 7.13 |
| $\sigma$ resultant span wise stress | LE | 5.17 | 6.01 |
| | TE | 6.75 | 7.00 |
| | Hi-c | 9.84 | 7.82 |
| | Midcv | 6.65 | 6.89 |
| Estimated Vibratory Capabilities | | | |
| $\sigma_{mean} = \sigma_c + \sigma_{lmi} + \sigma_{mmi}$ (ksi) ($\sigma_{thermal}$ neglected) | | 13.33 (HTE) | 49.30 (HLE) |
| Estimated $T_{HLE}$ (°F) | | 108 | 108 |
| Estimated Minimum Margin Vibratory Allowable Stress (ksisa) (Based on AISI 17-4 PH Stainless Steel average strength less three standard deviations) | | 68.8 | 53.9 |

TABLE V. KEY DETAIL DRAWING SUMMARY

| Drawing No. | Title |
|---|---|
| 4013098-116 | Hub, Tandem Vane - Stage 2 NASA HLMSFT |
| -117 | Shroud, Tandem Vane - Stage 2 NASA HLMSFT |
| -118 | Blade, Turbine - Stage 3F NASA HLMSFT Tandem |
| -119 | Blade, Turbine - Stage 3A NASA HLMSFT Tandem |
| -120 | Shroud, Tandem Turbine Blade - Stage 3 NASA HLMSFT |
| -121 | Blade Assembly, Turbine - Stage 3 NASA HLMSFT Tandem |
| -124 | Airfoil, Turbine Tandem Vane - Stage 2A NASA HLMSFT |
| -125 | Airfoil, Turbine Tandem Vane - Stage 2F NASA HLMSFT |
| -126 | Airfoil, Turbine Tandem Vane - Stage 3A NASA HLMSFT |
| -127 | Airfoil, Turbine Tandem Vane - Stage 3F NASA HLMSFT |
| -128 | Hub, Tandem Vane - Stage 3 NASA HLMSFT |
| -129 | Shroud, Tandem Vane - Stage 3, NASA HLMSFT |
| -130 | Vane Assembly, Stage 2 - Tandem NASA HLMSFT |
| -131 | Vane Assembly, Stage 3 - Tandem NASA HLMSFT |
| -132 | Disk, Tandem Rotor - Stage 3 NASA HLMSFT |
| -133 | Retainer, Tandem Blade - Stage 3 NASA HLMSFT |
| -134 | Ring, Tandem Torque - Stage 3 NASA HLMSFT |
| -135 | Housing Assembly, Tandem Vane - Stage 2 NASA HLMSFT |
| -136 | Housing Assembly, Tandem Vane - Stage 2 NASA HLMSFT |
| -140 | NASA HLMSFT Test Assembly, Tandem Blading |

TABLE V. KEY DETAIL DRAWING SUMMARY (Concluded)

| Precision Master No. | Title |
|---|---|
| 4012241-962 | Vane, Tandem, Stage 2 Forward |
| -963 | Stackup, Tandem Vane, Stage 2 Forward |
| -964 | Vane, Tandem, Stage 2 Aft |
| -965 | Stackup, Tandem Vane, Stage 2 Aft |
| -966 | Vane, Tandem, Stage 3 Forward |
| -967 | Stackup, Tandem Vane, Stage 3 Forward |
| -968 | Vane, Tandem, Stage 3 Aft |
| -969 | Stackup, Tandem Vane, Stage 3 Aft |
| -970 | Blade, Tandem, Stage 3 Forward |
| -971 | Stackup, Tandem Blade, Stage 3 Forward |
| -972 | Blade, Tandem, Stage 3 Aft |
| -973 | Stackup, Tandem Blade, Stage 3 Aft |

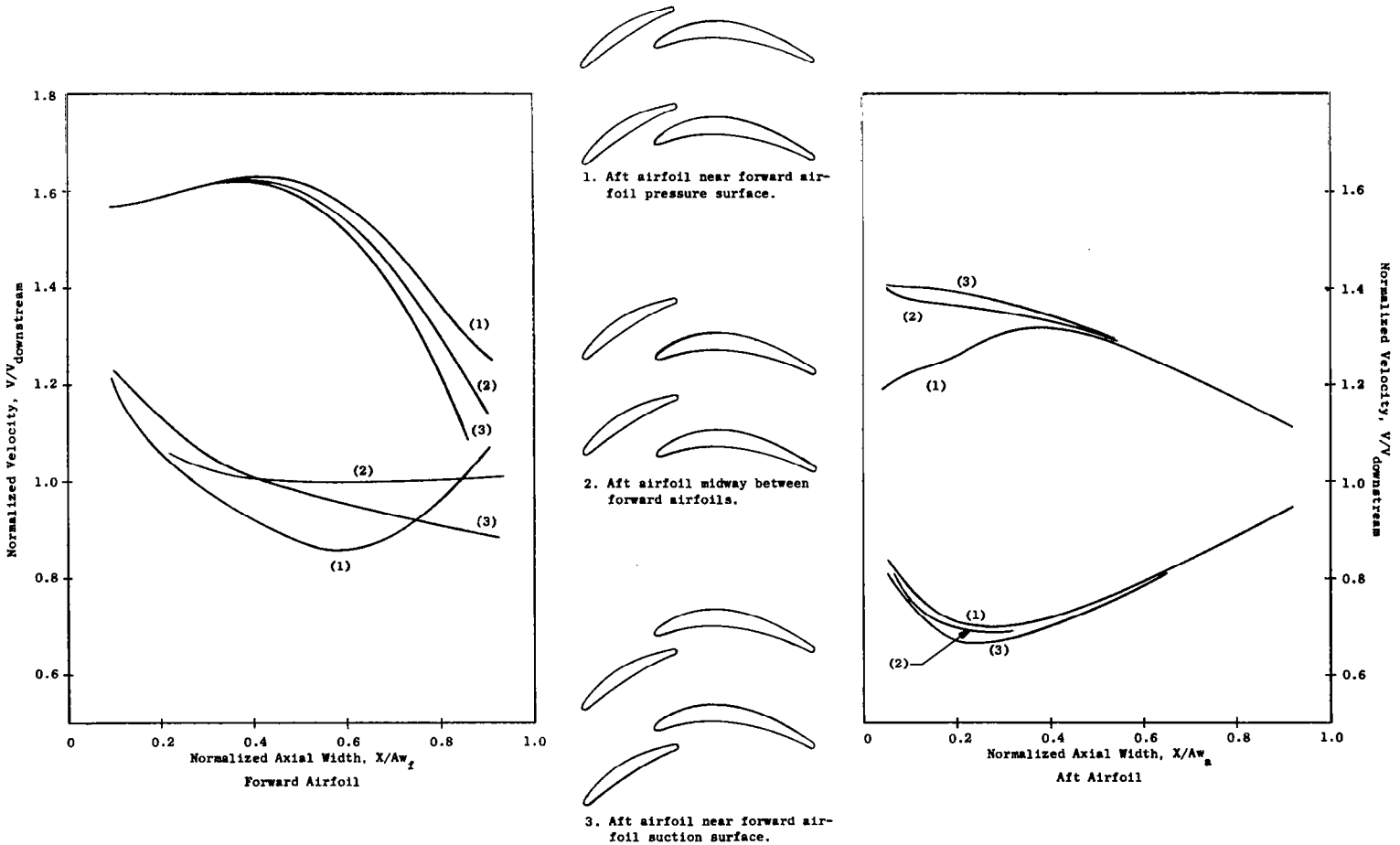


**Figure 1. Effect of Tangential Spacing on Velocity Distribution.**

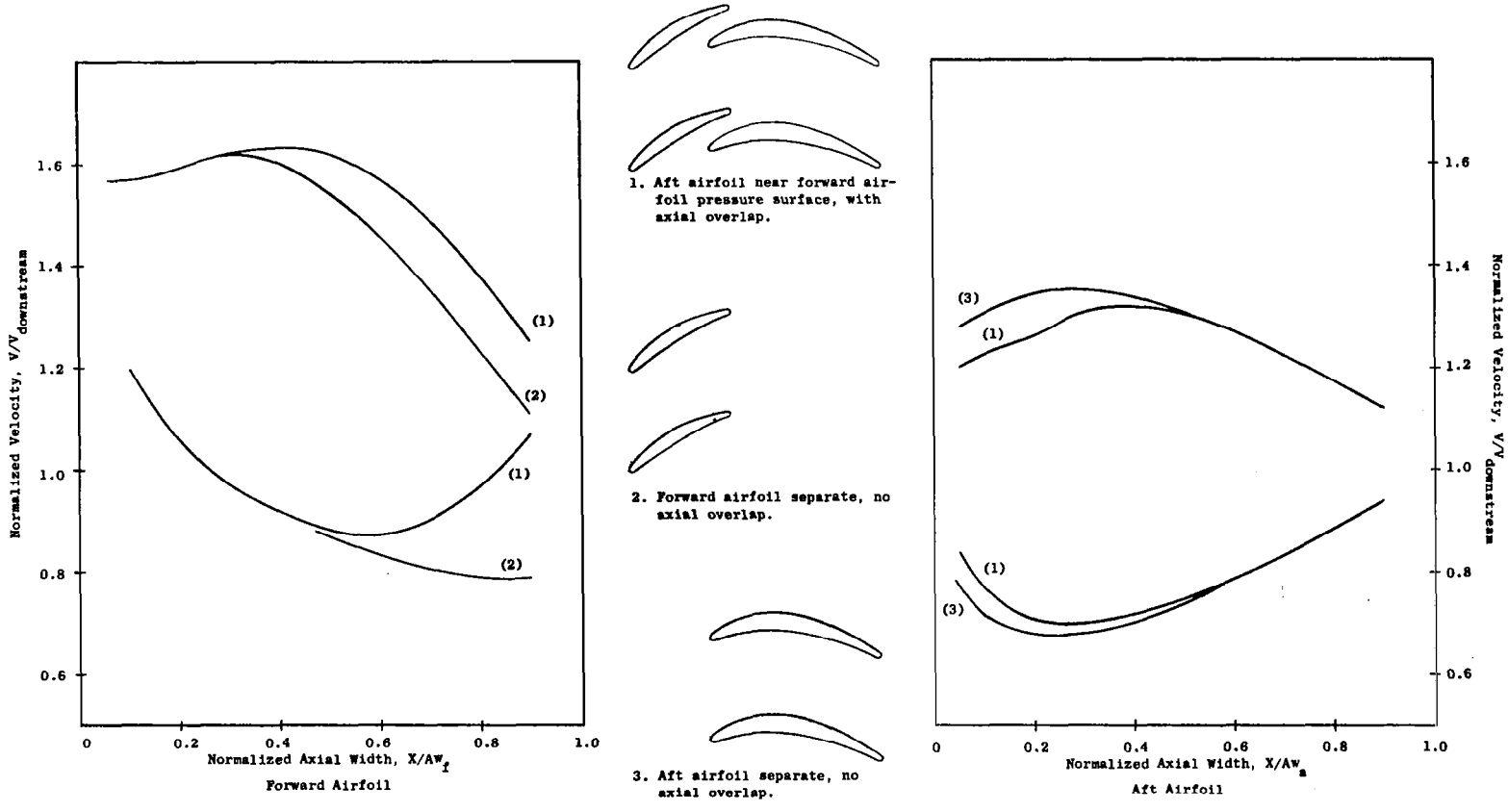


**Figure 2. Effect of Axial Spacing on Velocity Distribution.**

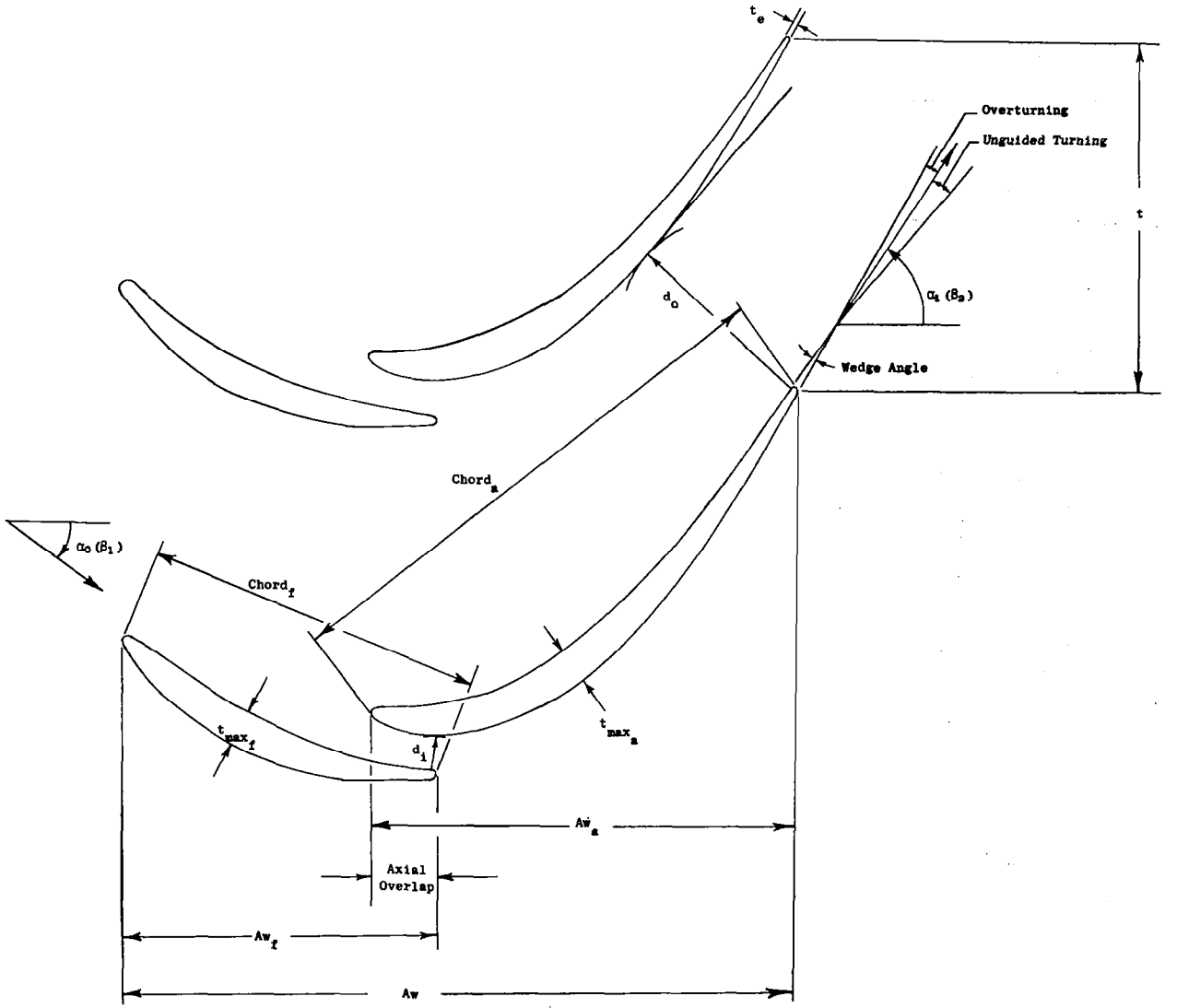


Figure 3. Design Data Nomenclature.

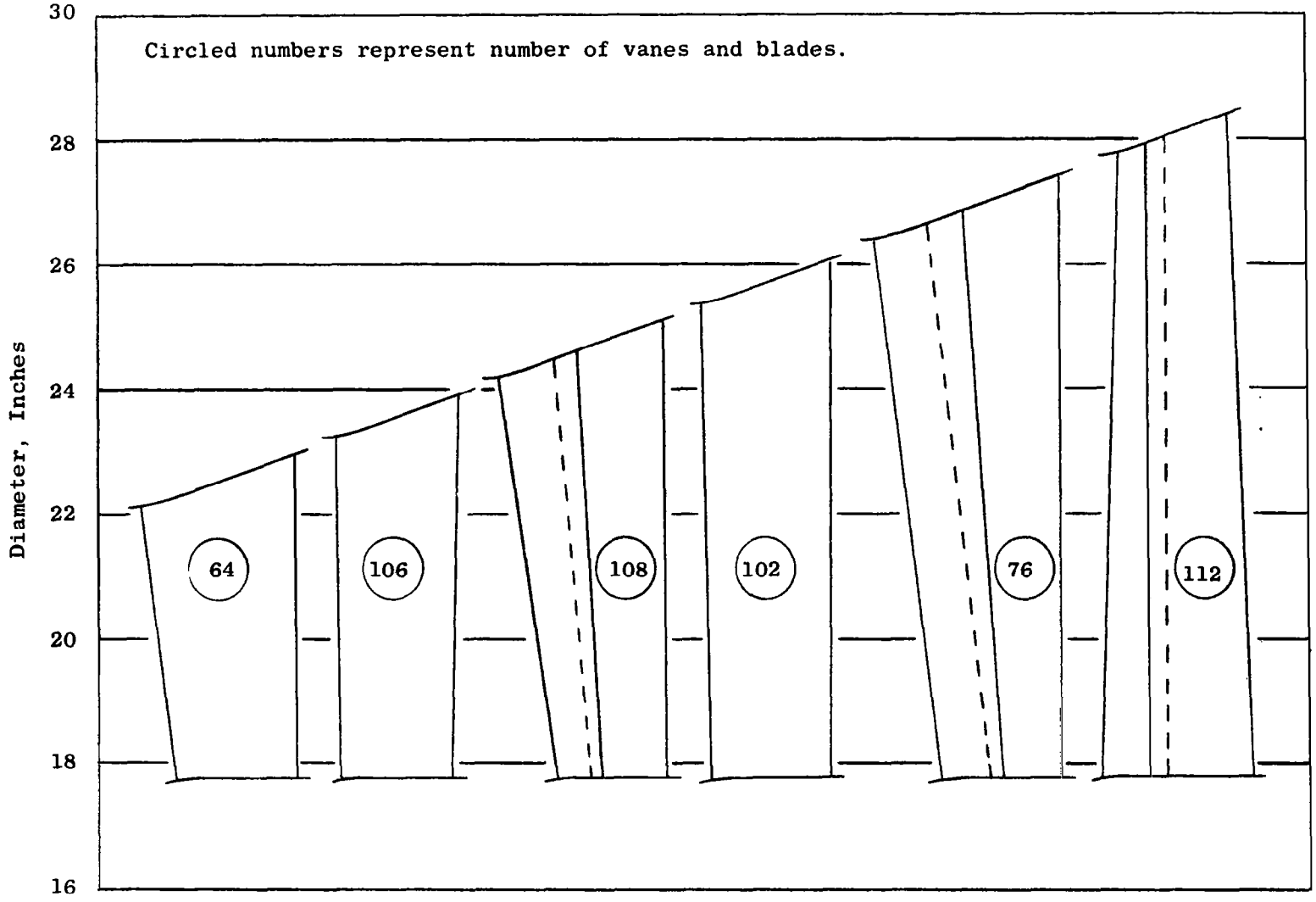


Figure 4. Aerodynamic Flowpath.

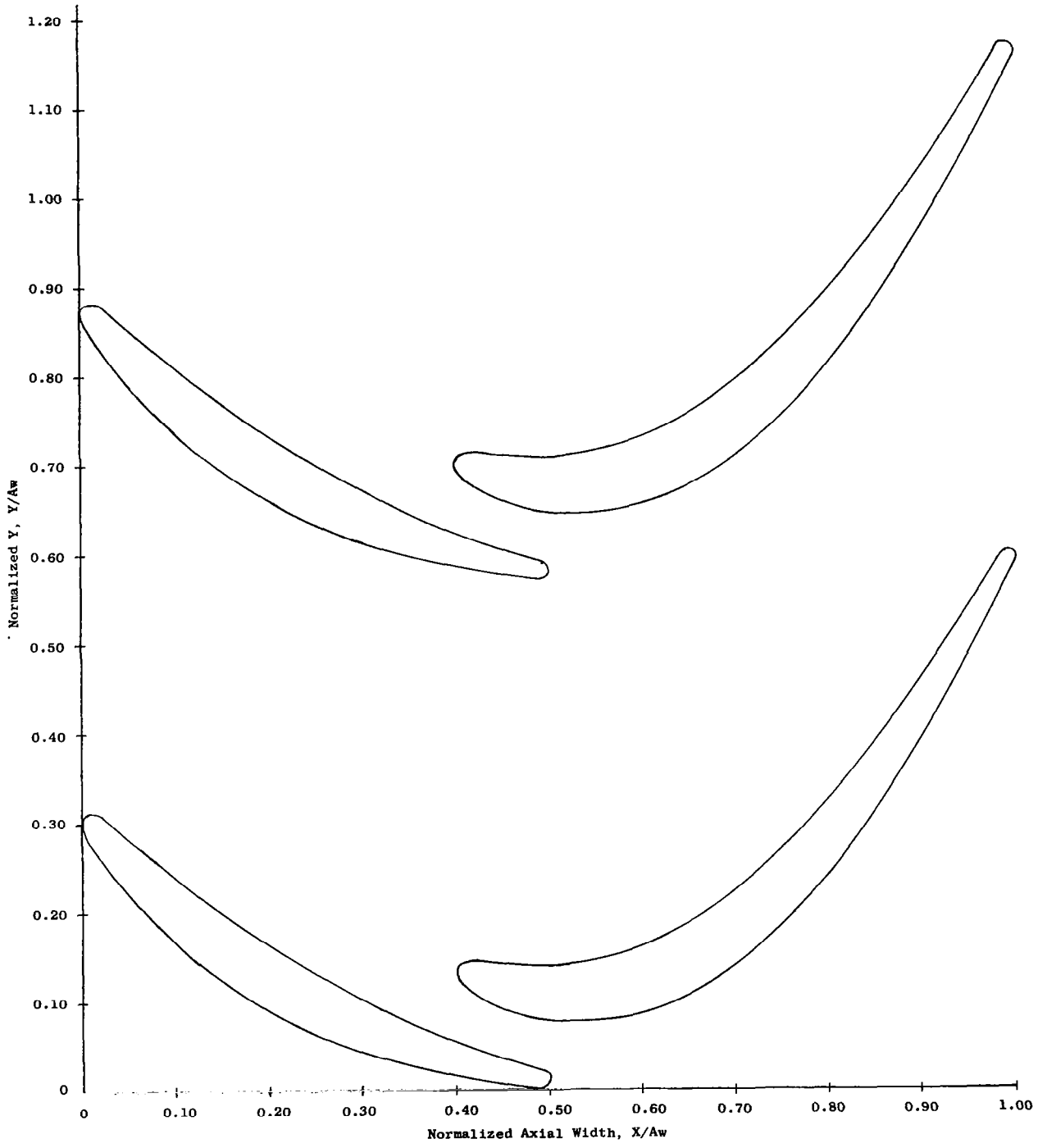


**Figure 5. Stage Two Tandem Vane Hub Airfoil Flowpath.**

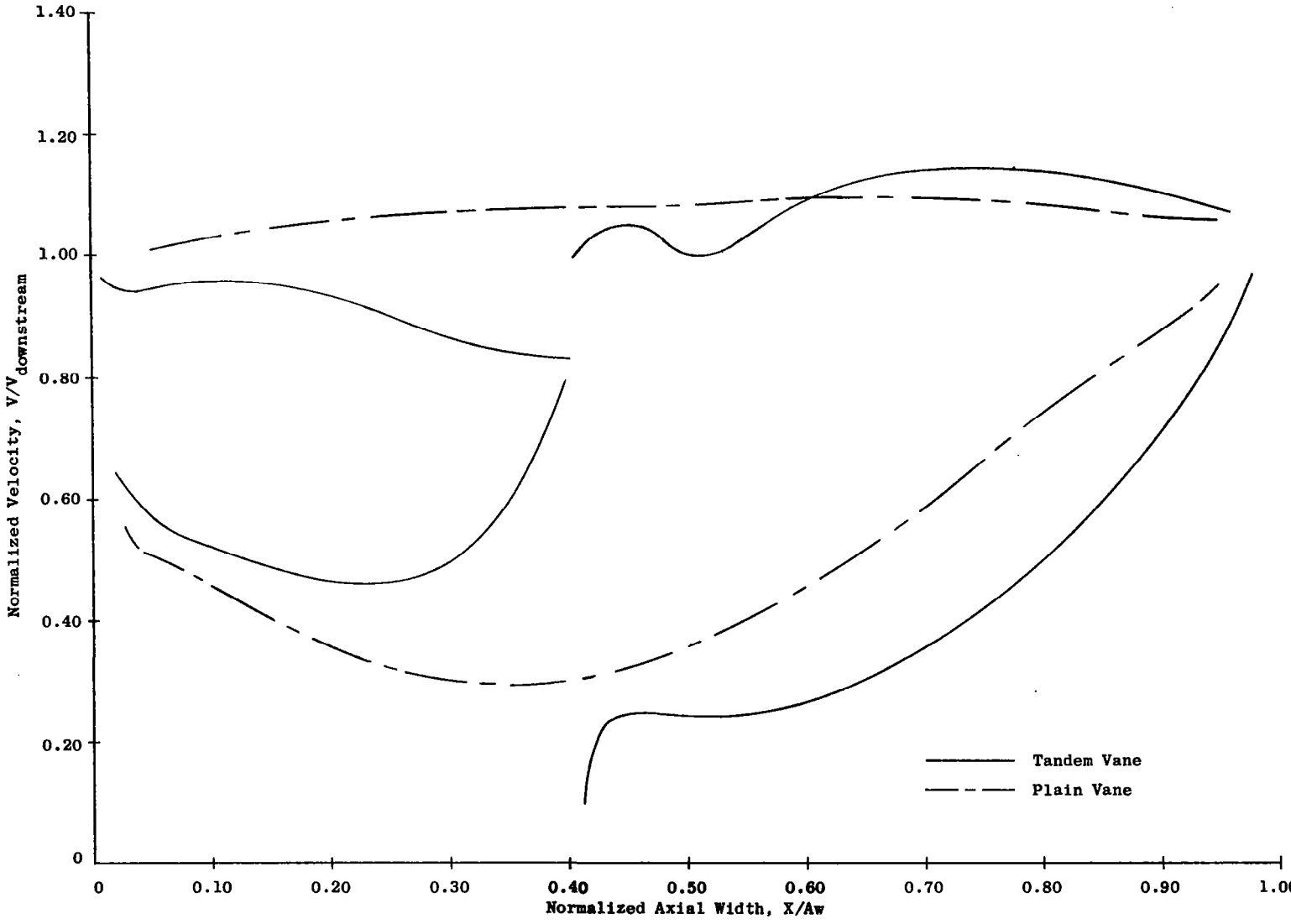


Figure 6. Stage Two Vane Hub Velocity Distribution.

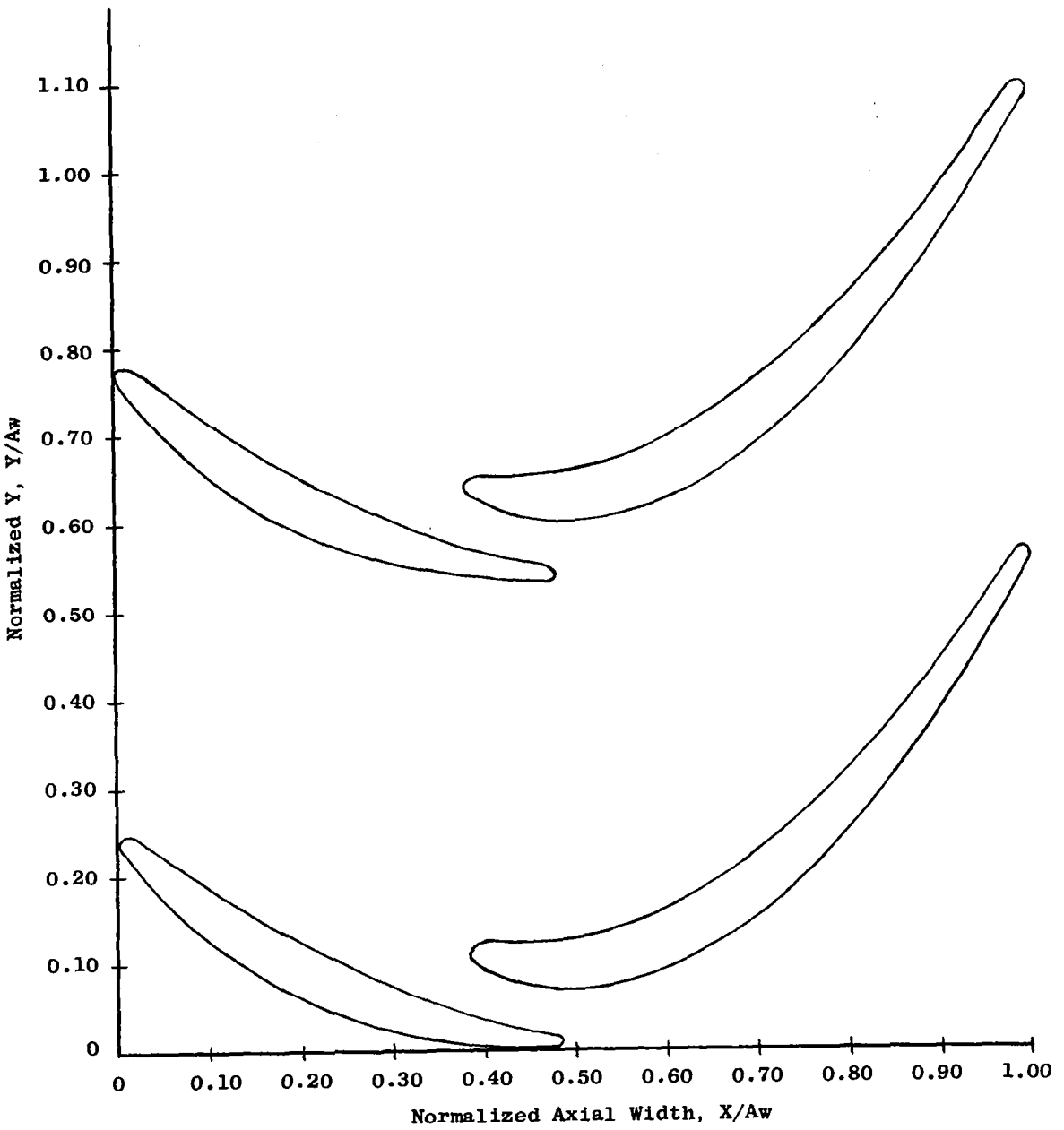


Figure 7. Stage Two Tandem Vane Pitch Airfoil Flowpath.

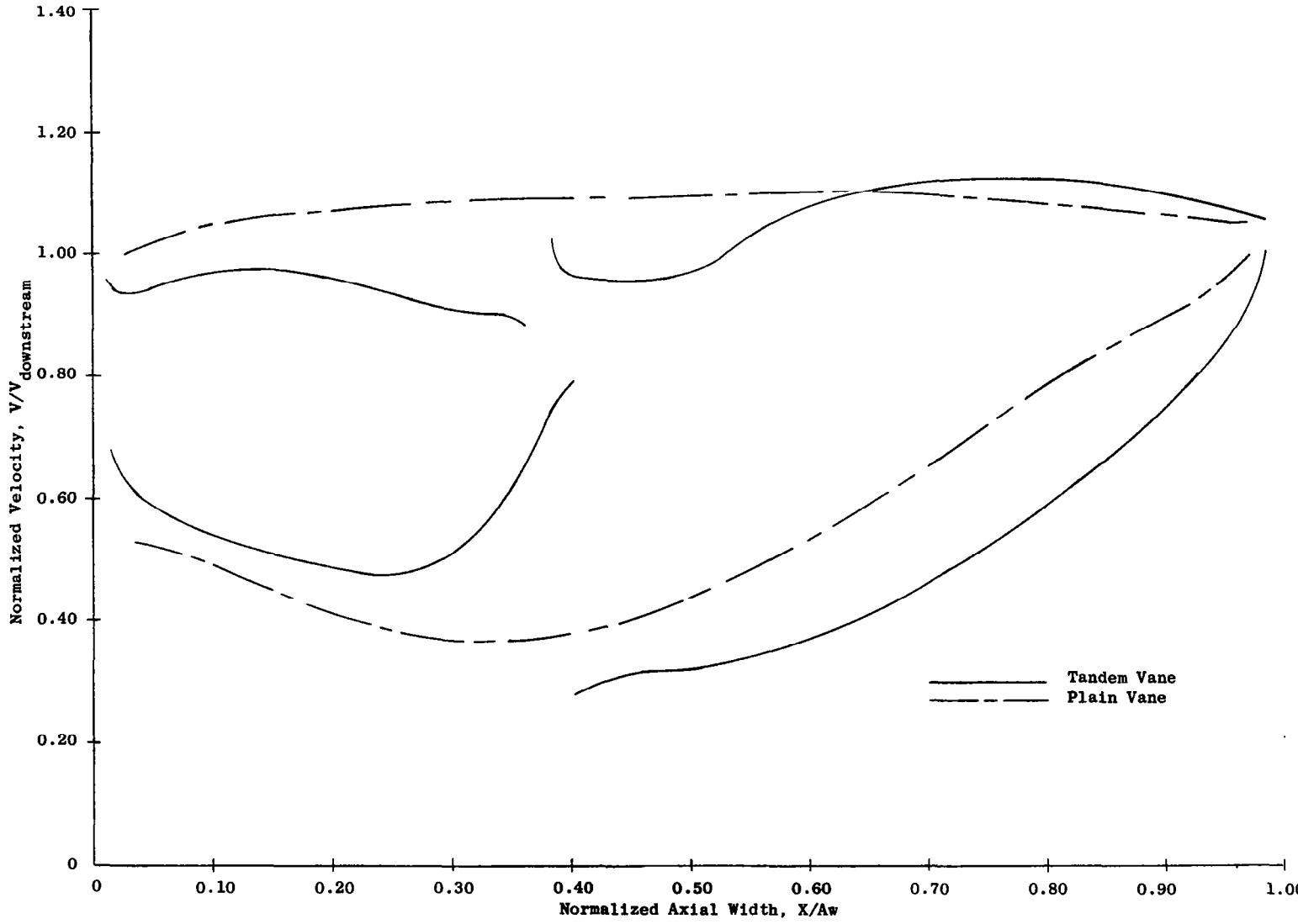


Figure 8. Stage Two Vane Pitch Velocity Distribution.

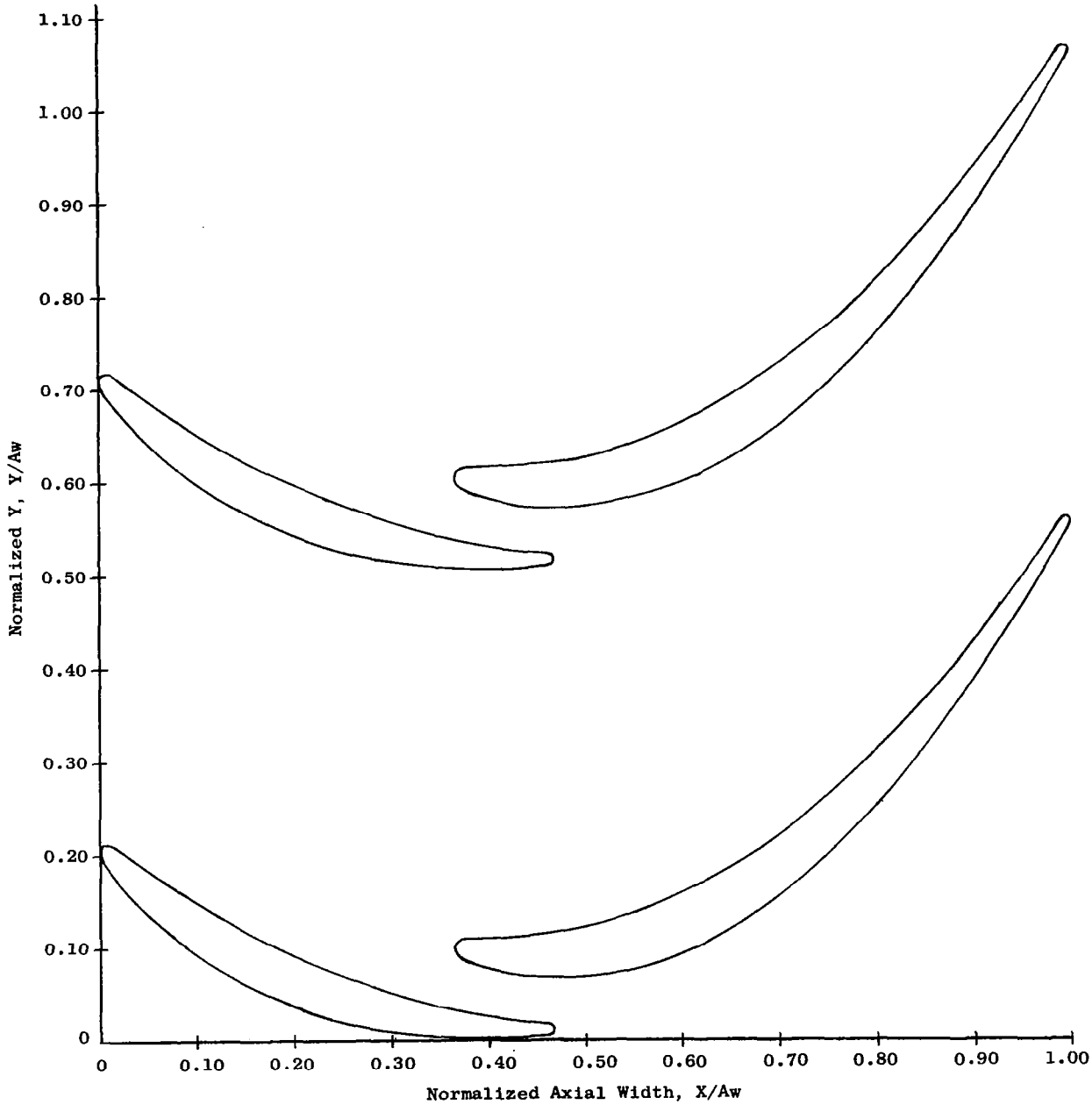


Figure 9. Stage Two Tandem Vane Tip Airfoil Flowpath.

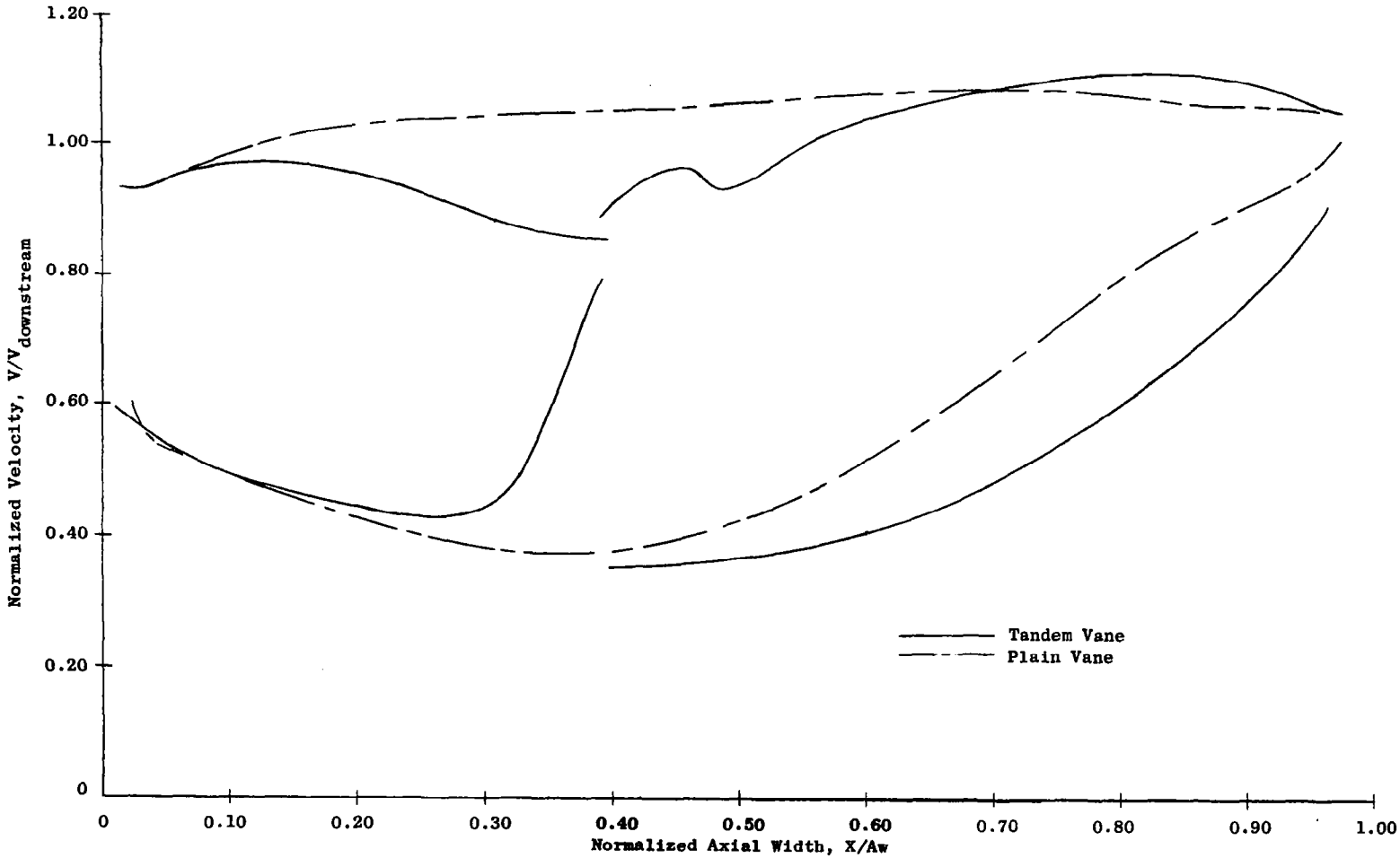


Figure 10. Stage Two Vane Tip Velocity Distribution.

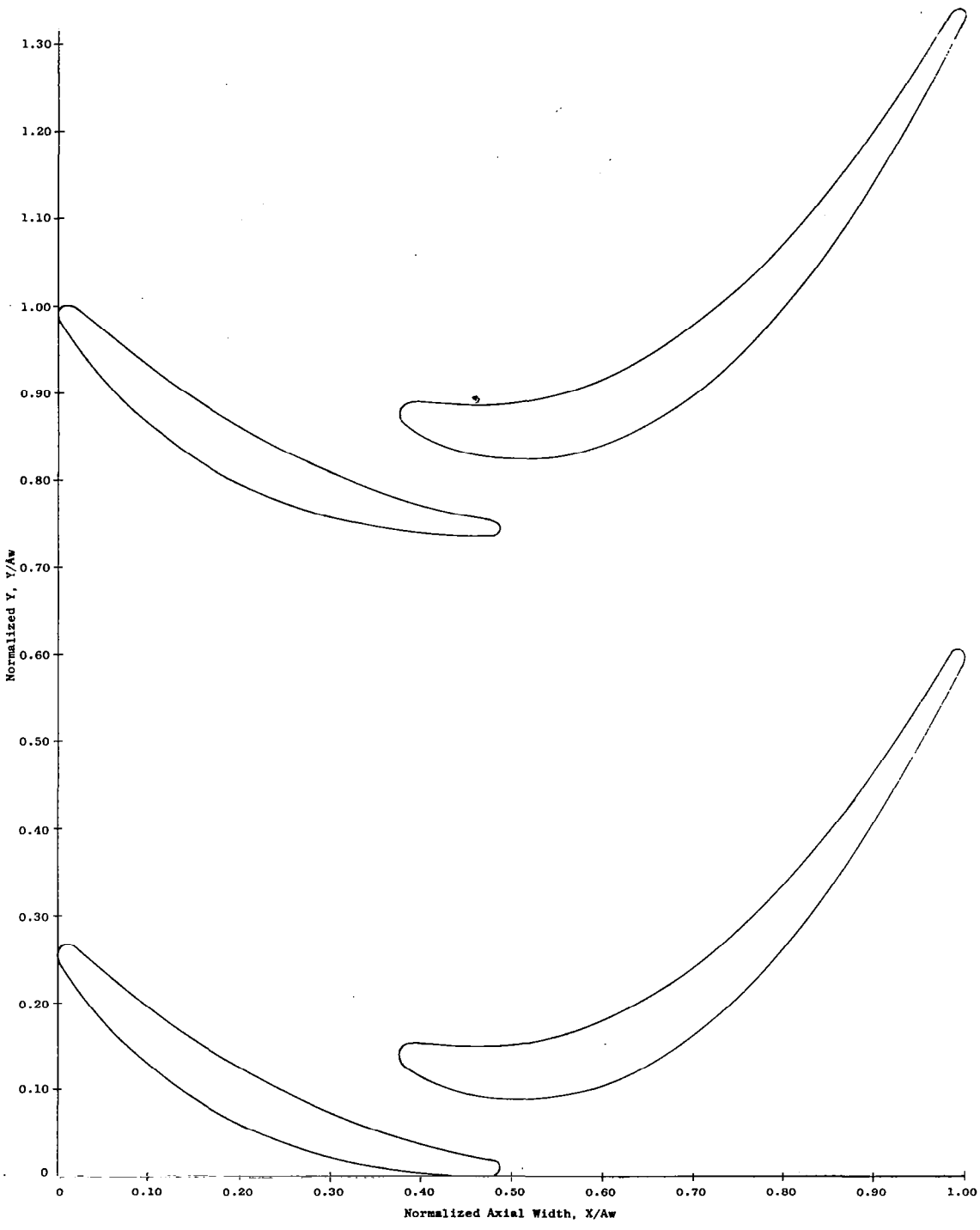


**Figure 11. Stage Three Tandem Vane Hub Airfoil Flowpath.**

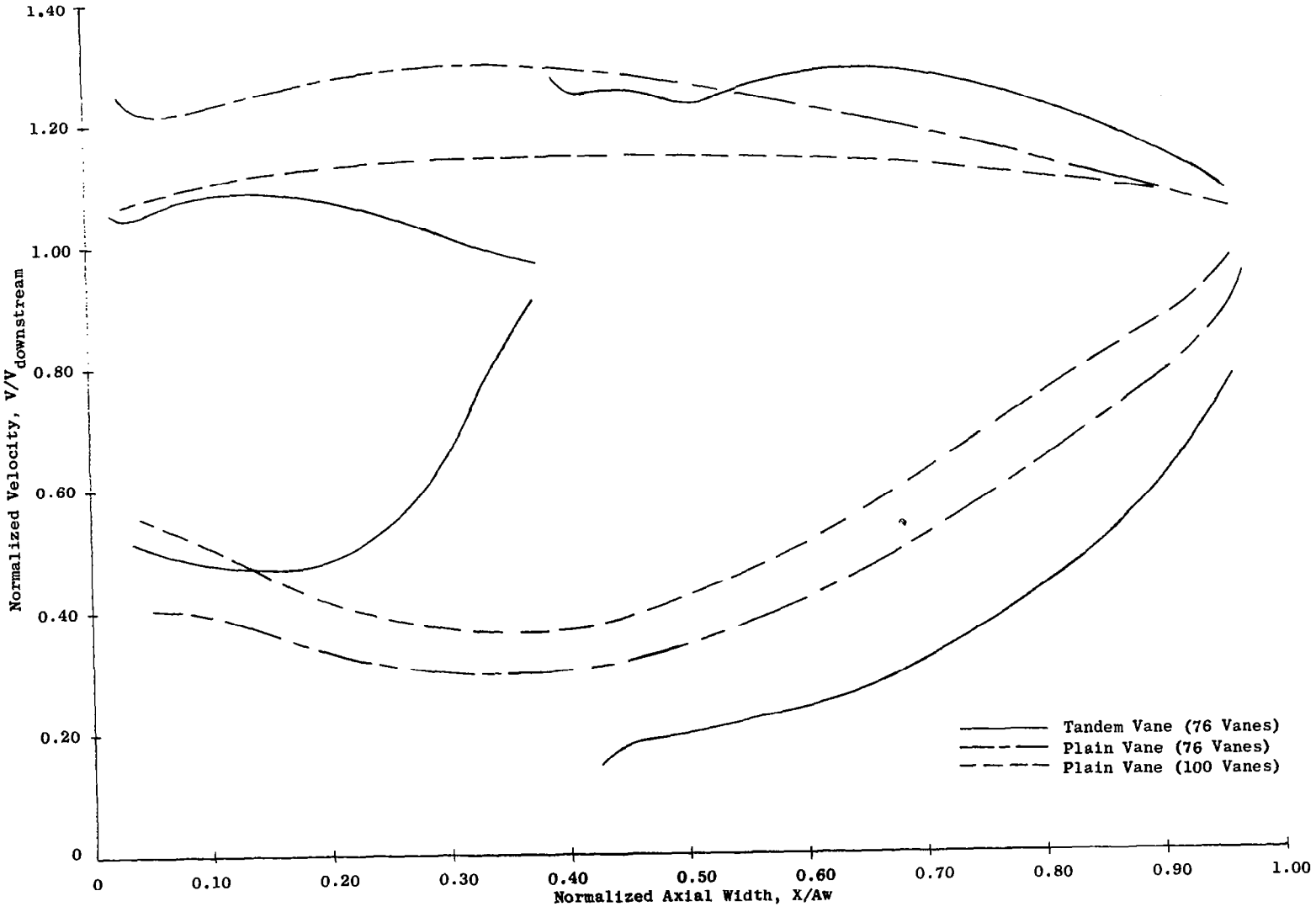


Figure 12. Stage Three Vane Hub Velocity Distribution.

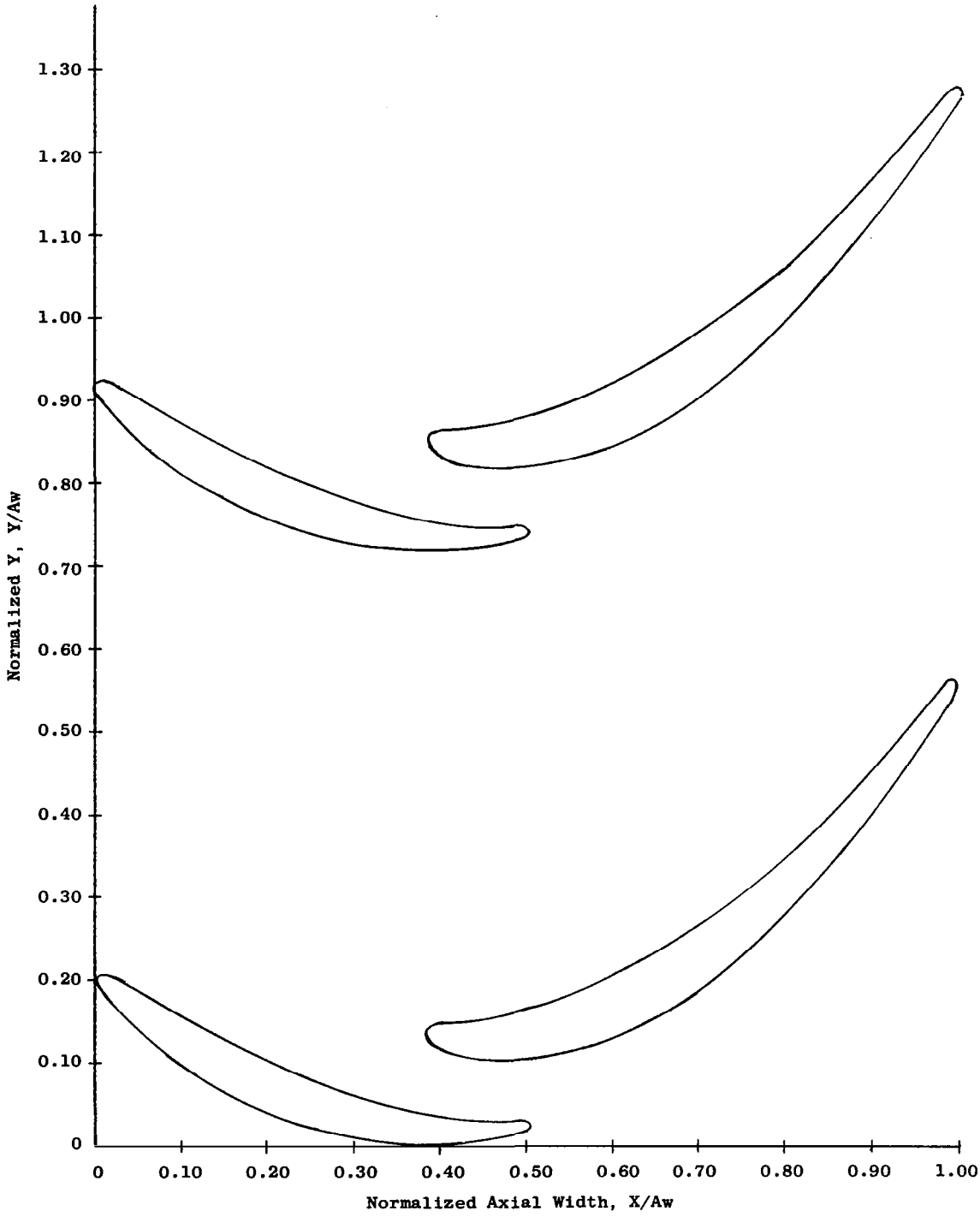


Figure 13. Stage Three Tandem Vane Pitch Airfoil Flowpath.

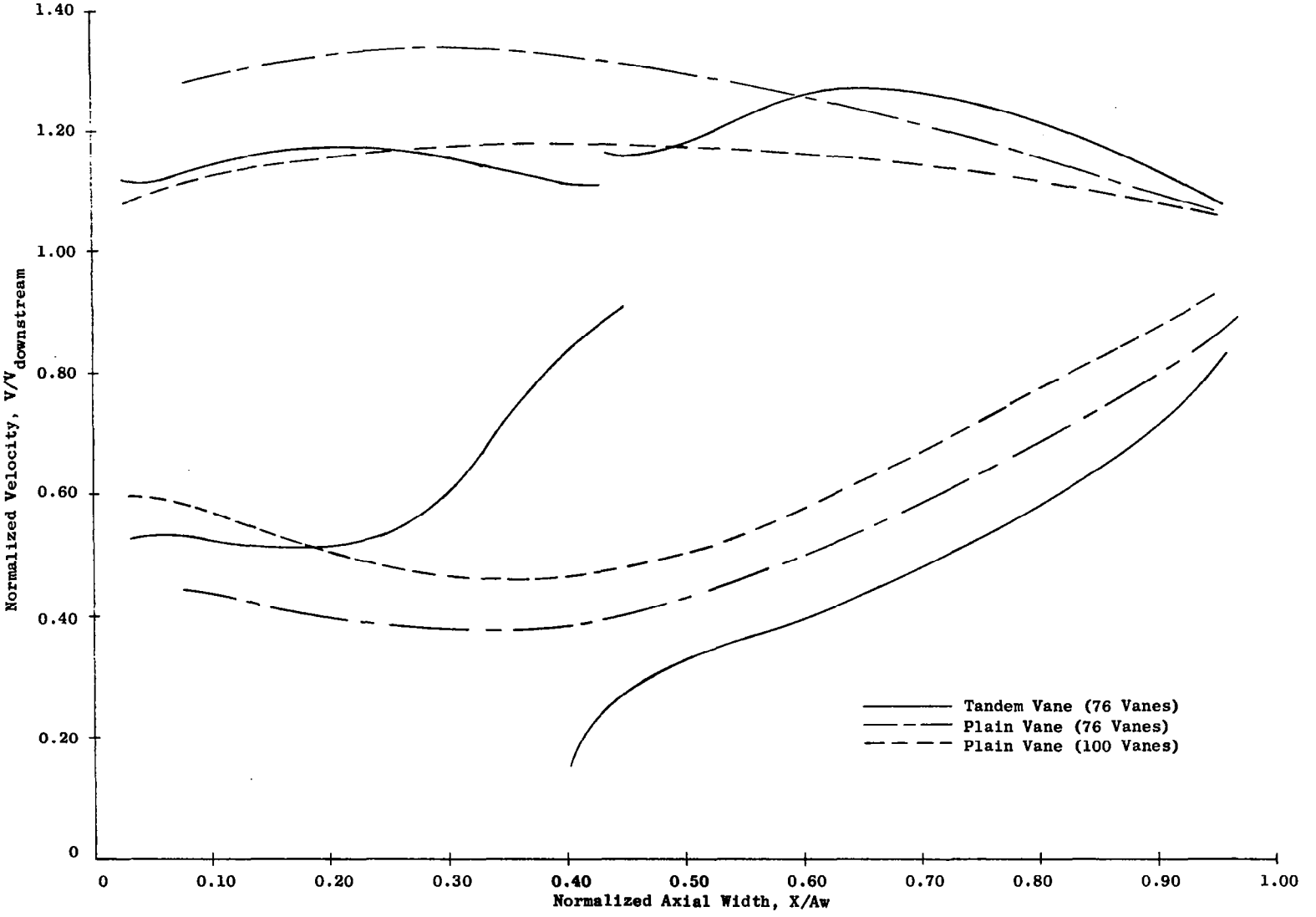


Figure 14. Stage Three Vane Pitch Velocity Distribution.

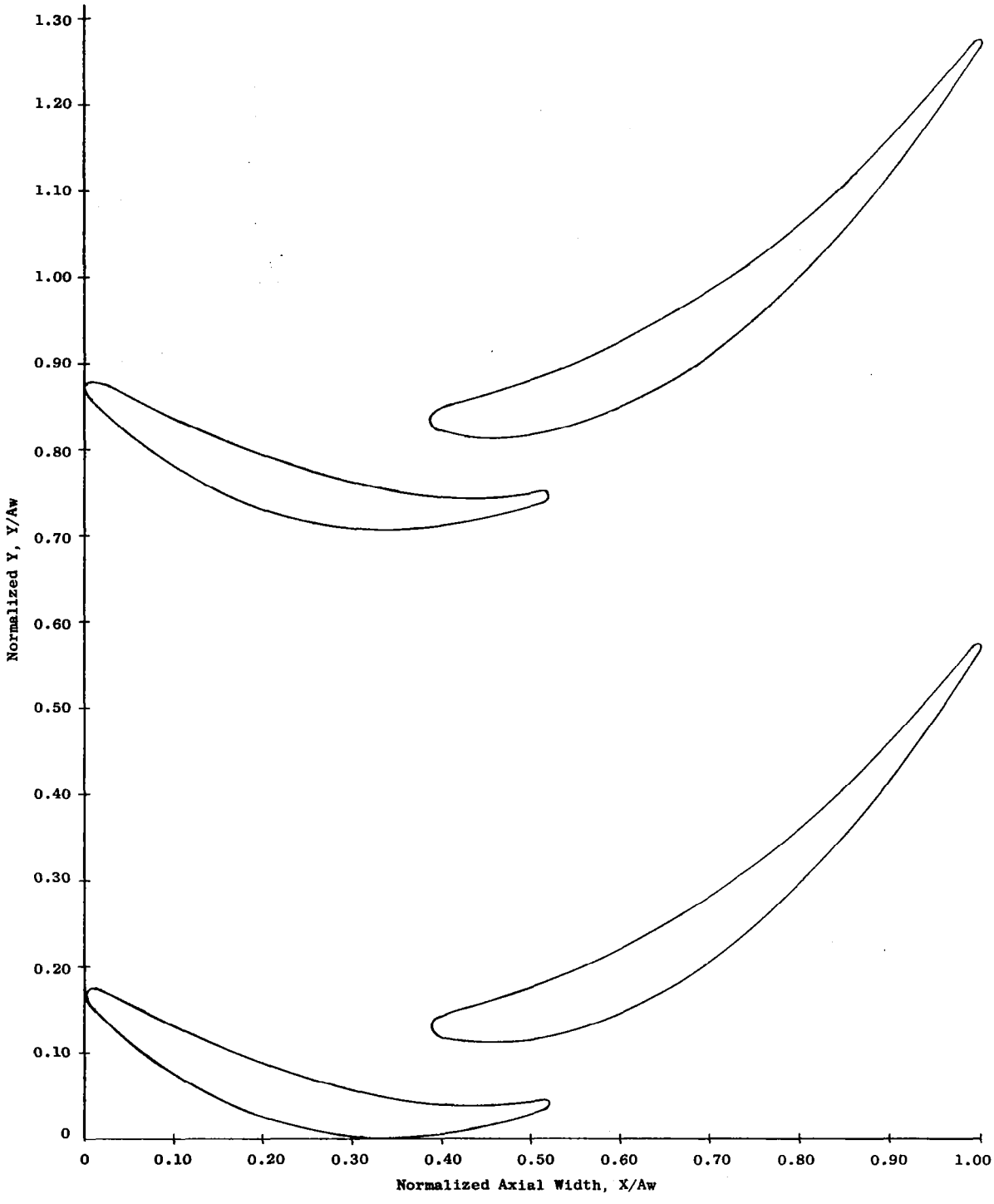


Figure 15. Stage Three Tandem Vane Tip Airfoil Flowpath.

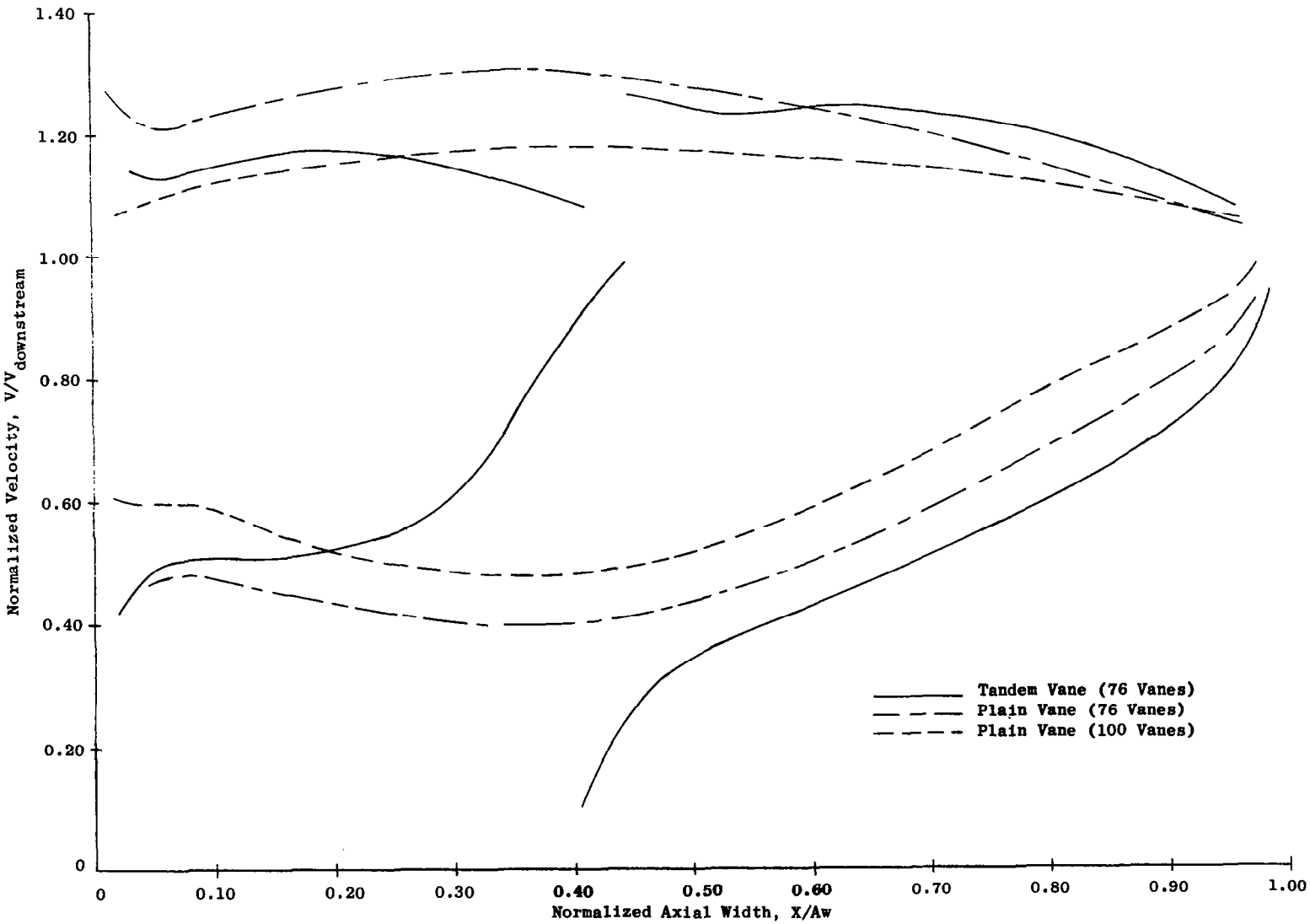


Figure 16. Stage Three Vane Tip Velocity Distribution.

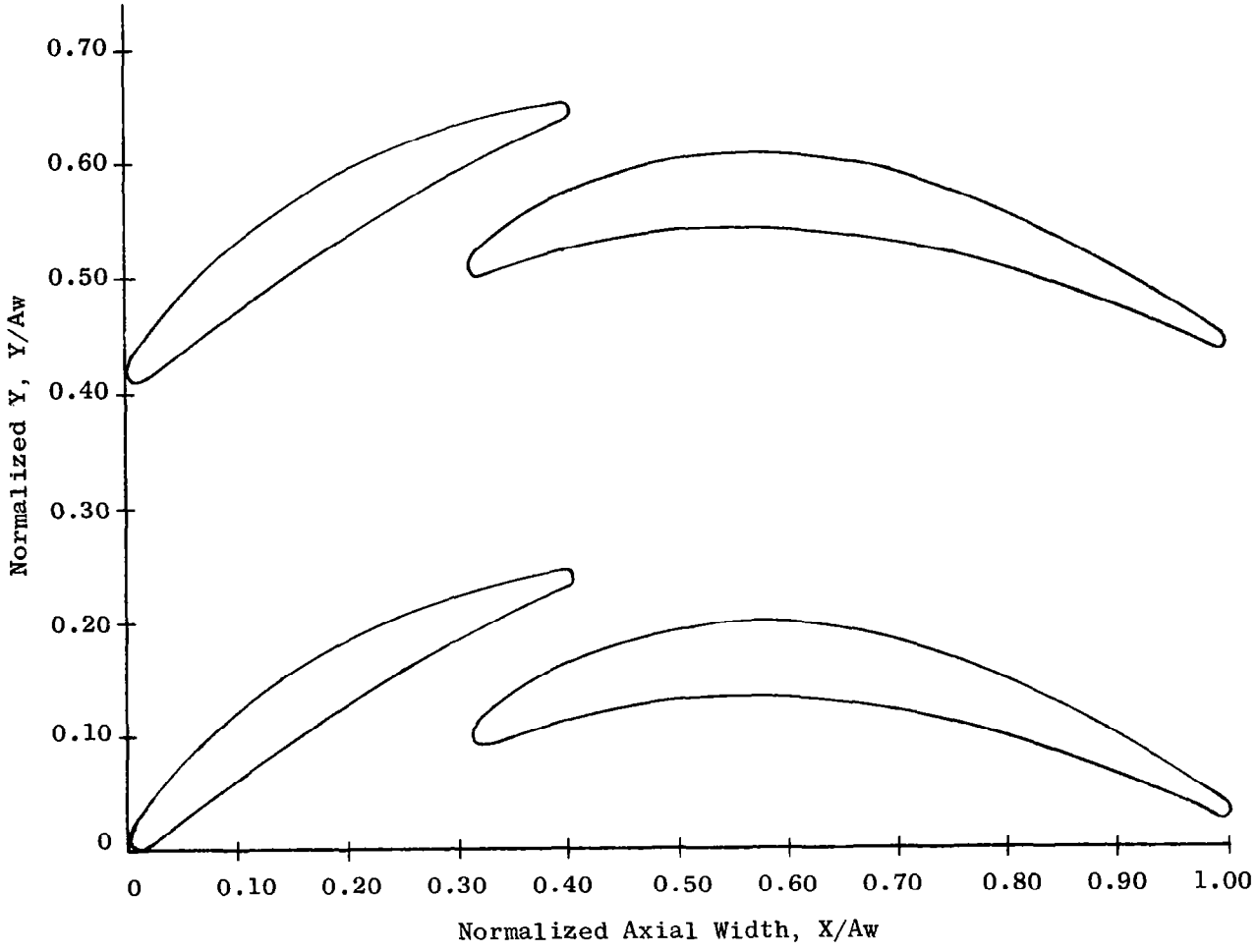


Figure 17. Stage Three Tandem Blade Hub Airfoil Flowpath.

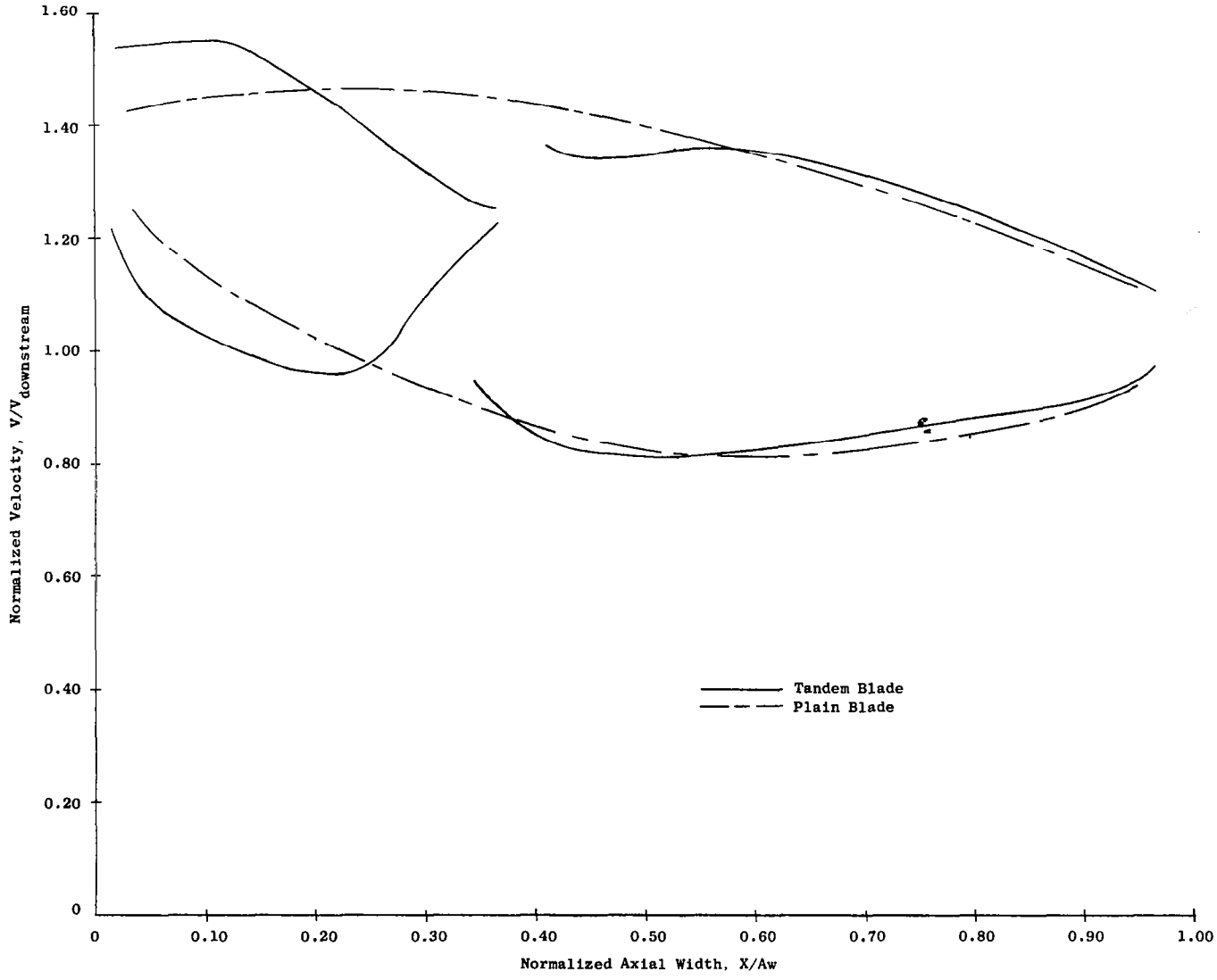


Figure 18. Stage Three Blade Hub Velocity Distribution.

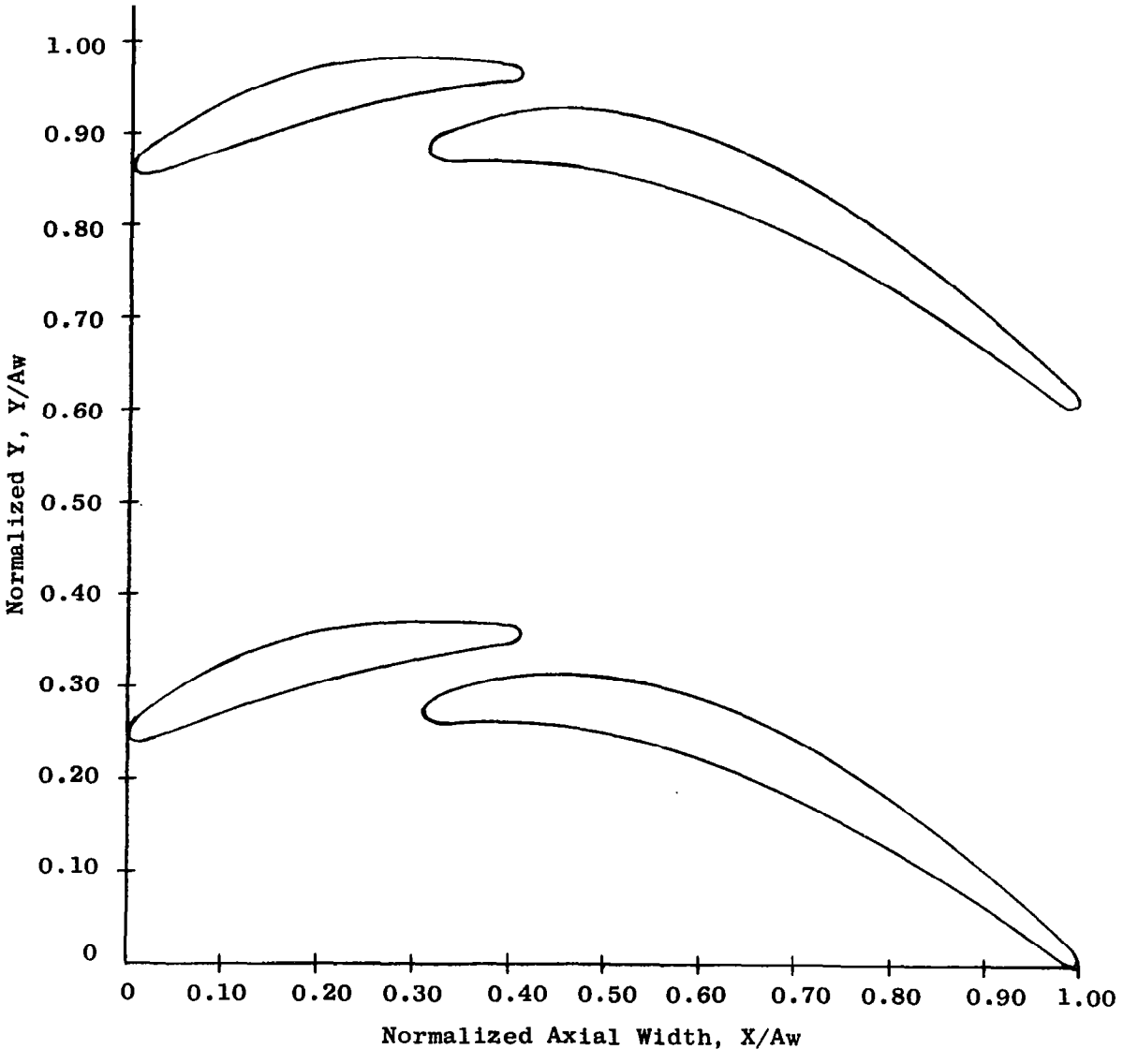


Figure 19. Stage Three Tandem Blade Pitch Airfoil Flowpath.

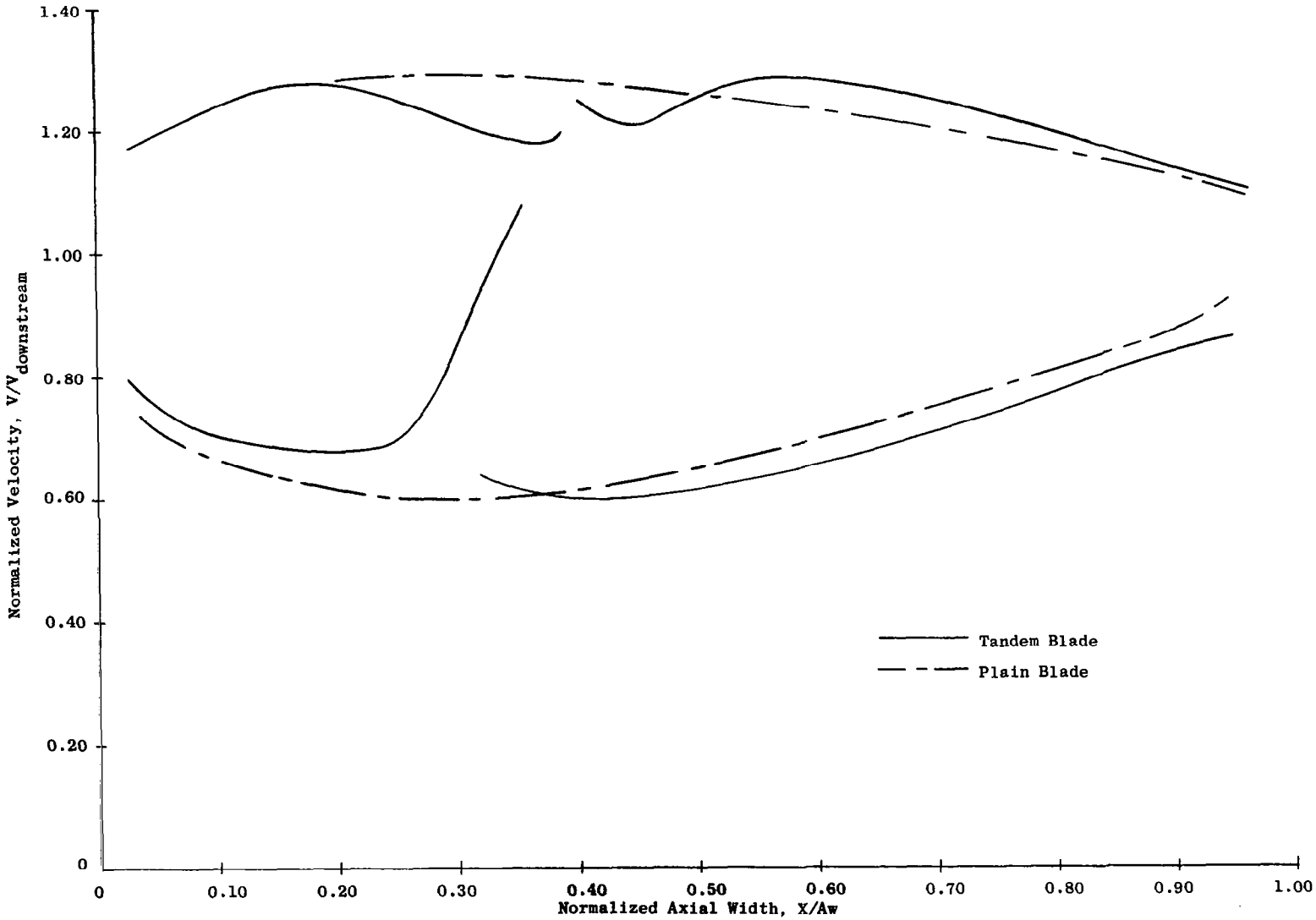


Figure 20. Stage Three Blade Pitch Velocity Distribution.

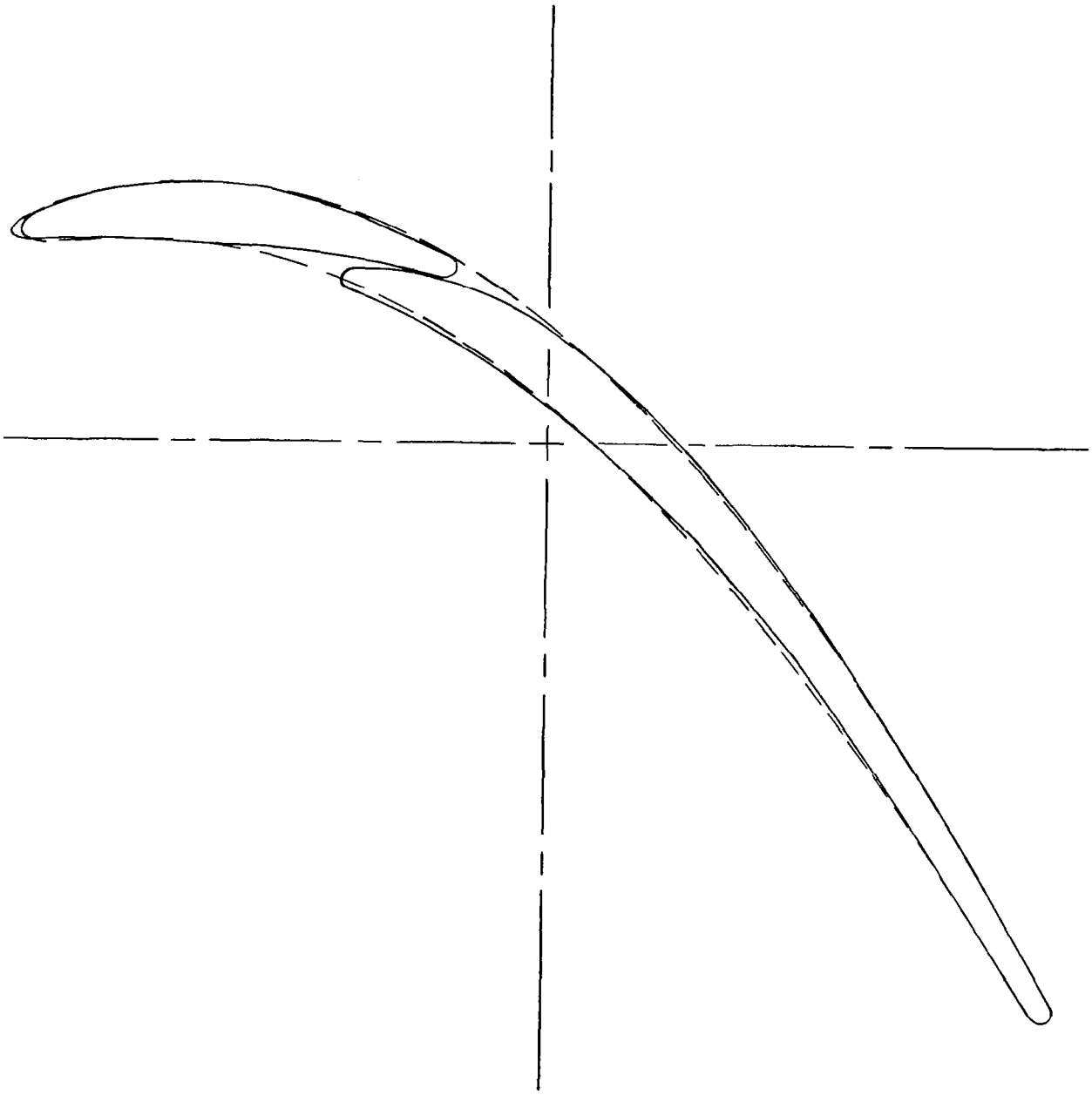

Figure 21. Stage Three Tandem Blade Tip Compared to Stage Three Plain Blade Tip.

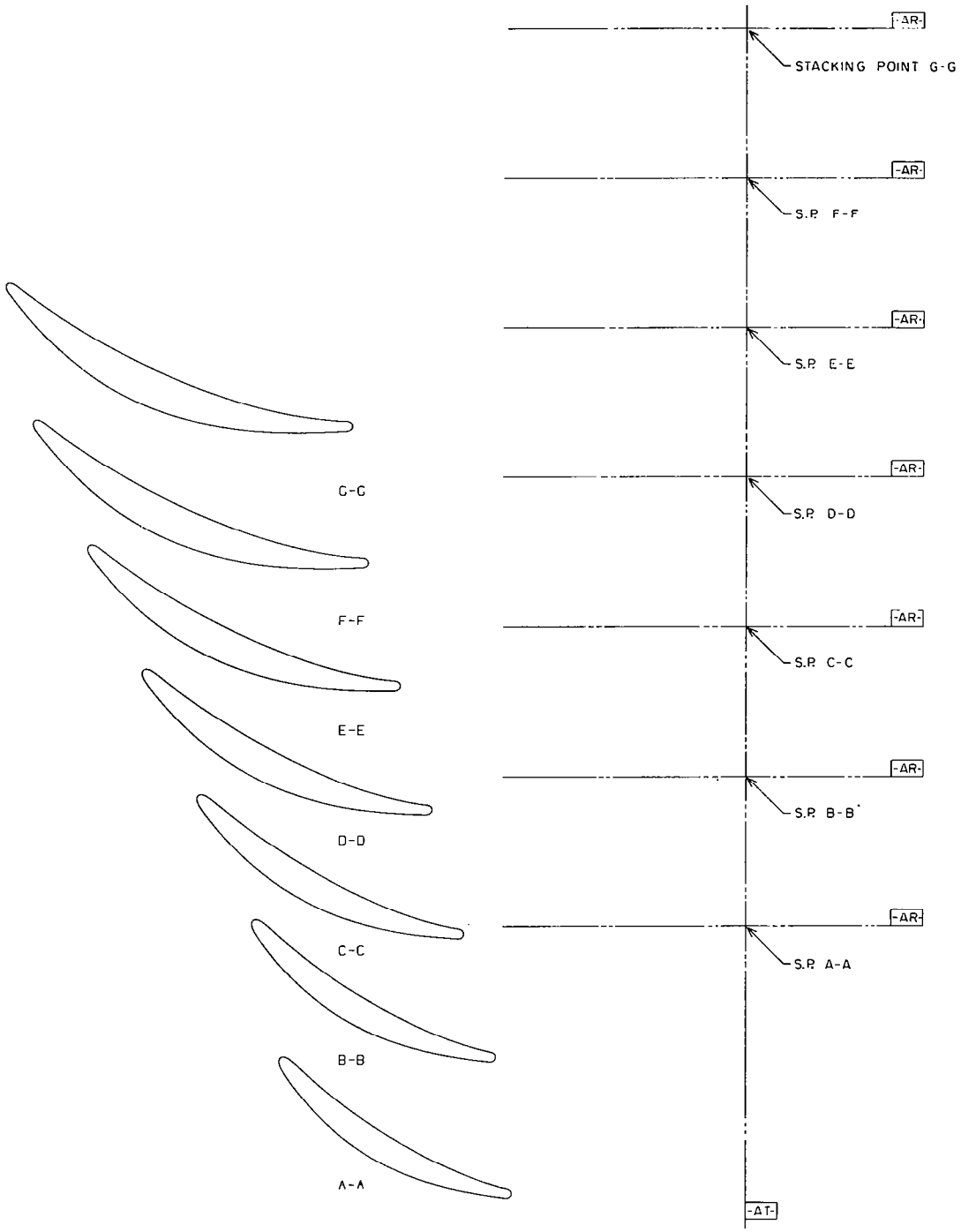


**Figure 22. Stage Two Forward Tandem Vane Precision Master (4012241-962).**

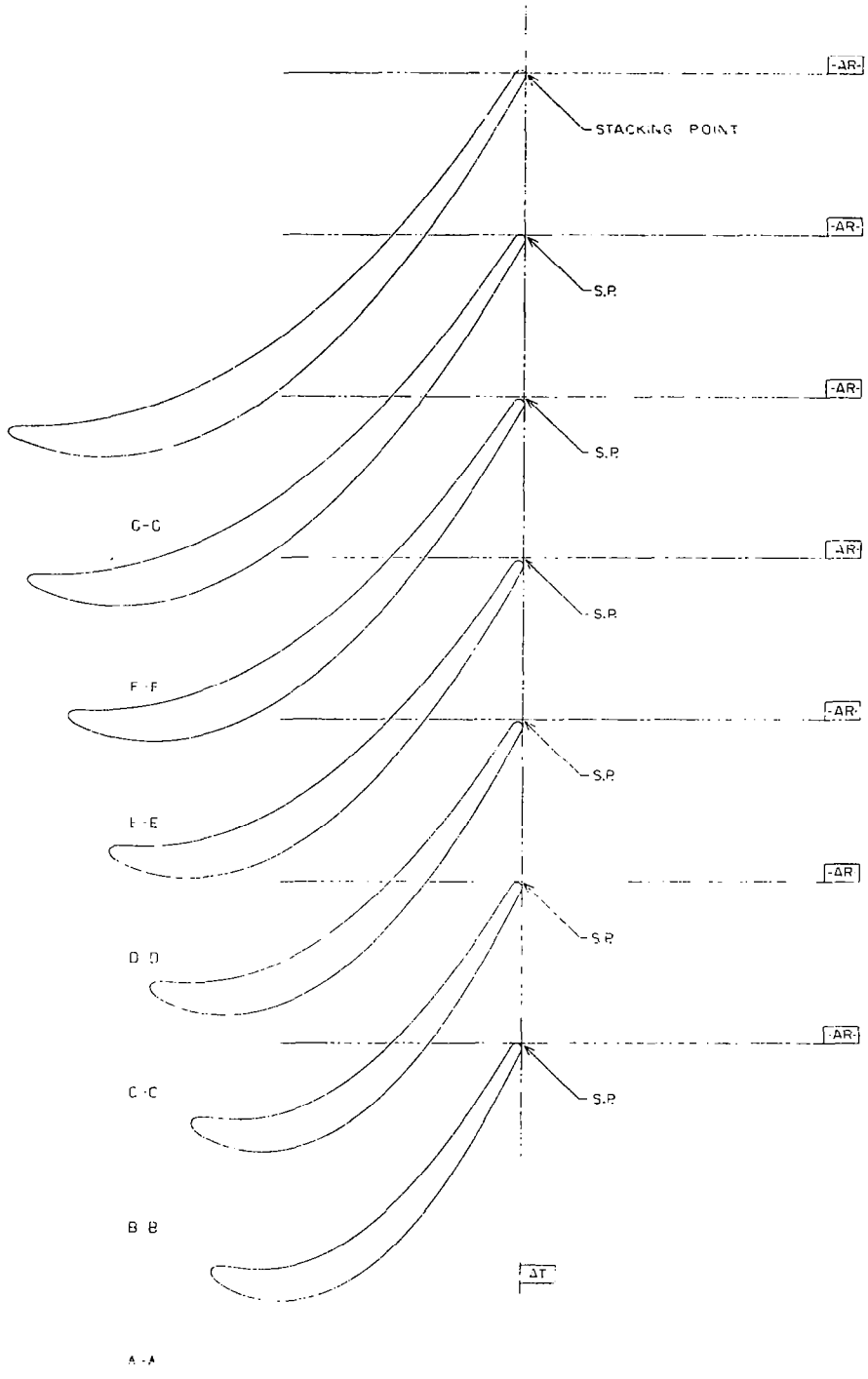


**Figure 23. Stage Two Aft Tandem Vane Precision Master (4012241-964).**

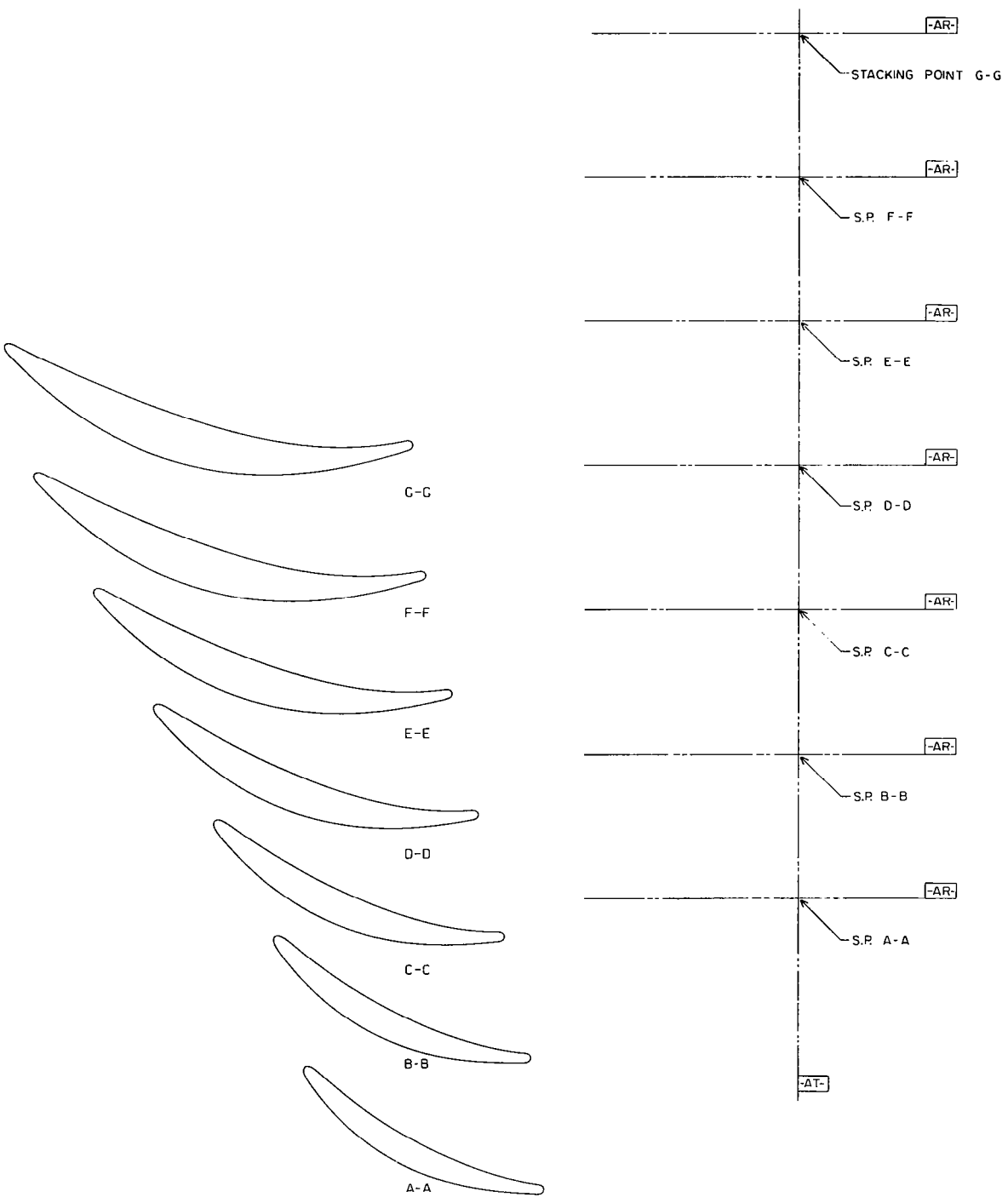


**Figure 24. Stage Three Forward Tandem Vane Precision Master (4012241-966).**

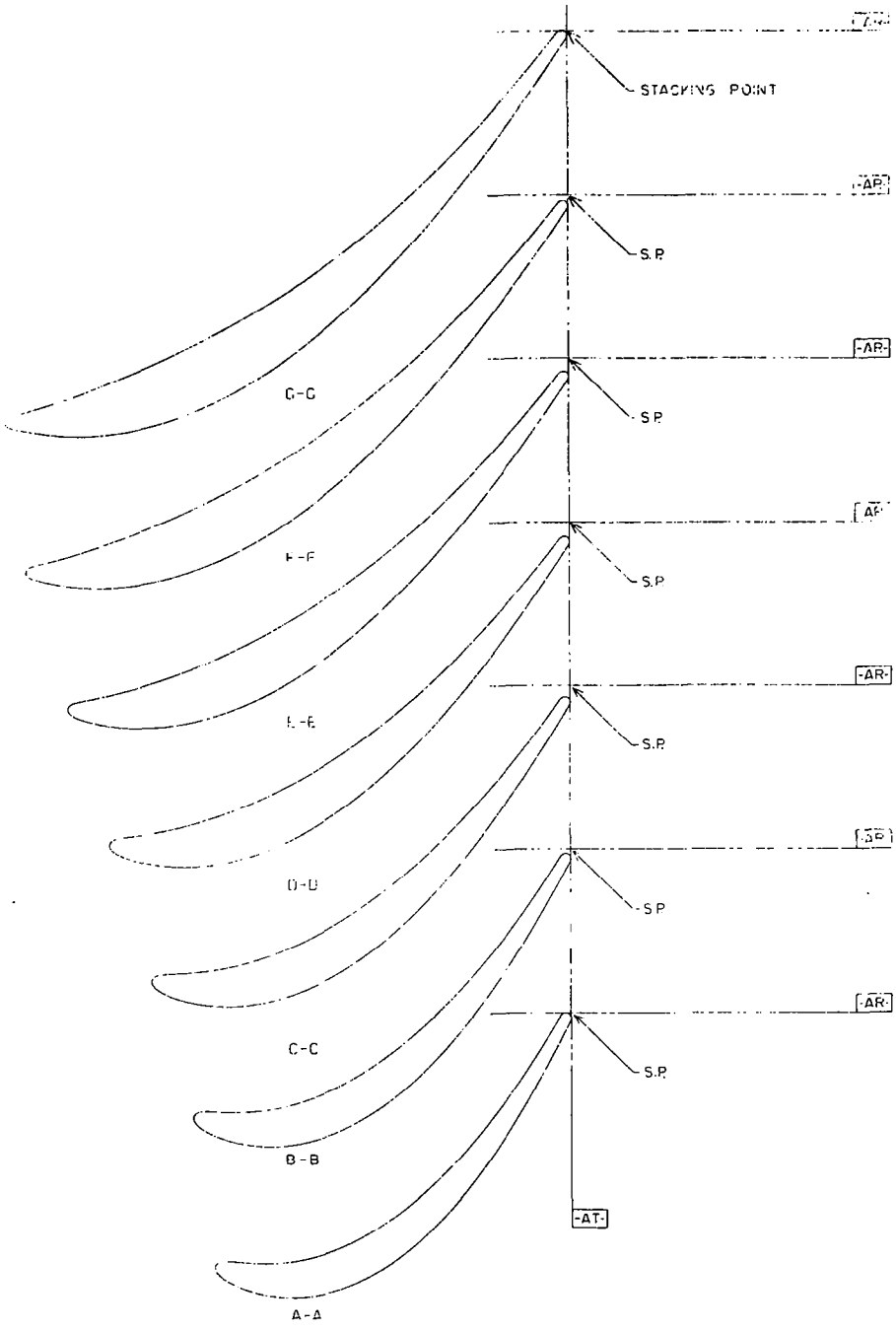


**Figure 25. Stage Three Aft Tandem Vane Precision Master (4012241-968).**

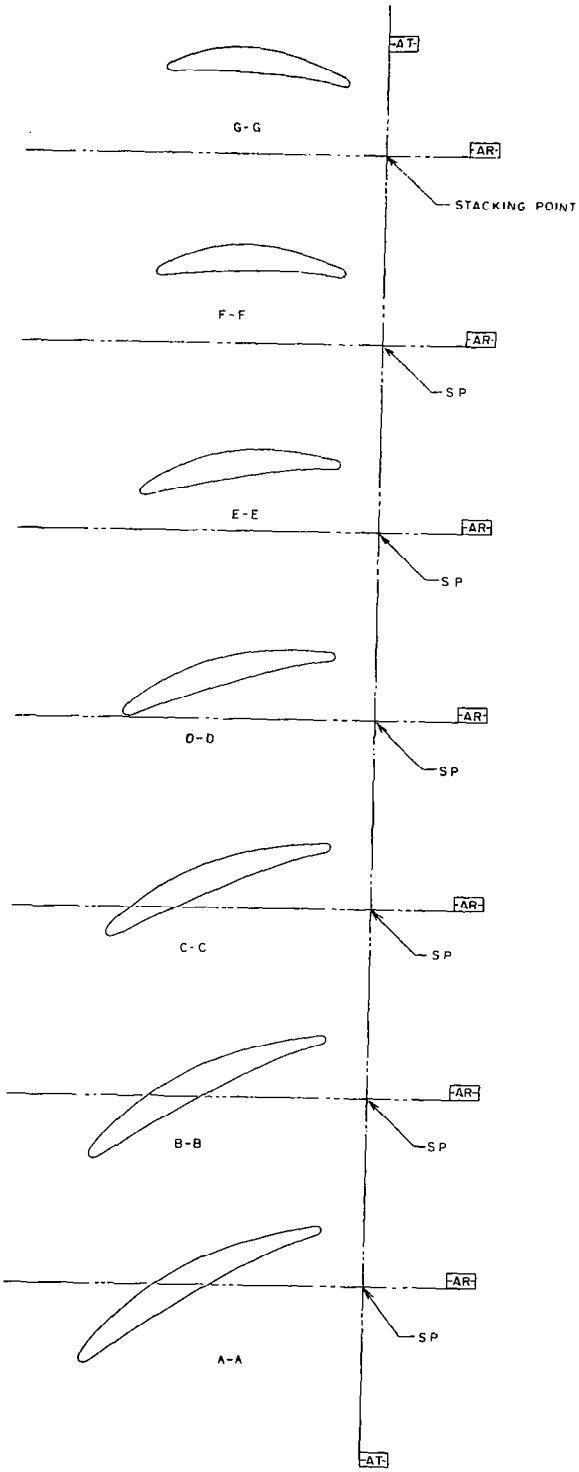


**Figure 26. Stage Three Forward Tandem Blade Precision Master (4012241-970).**

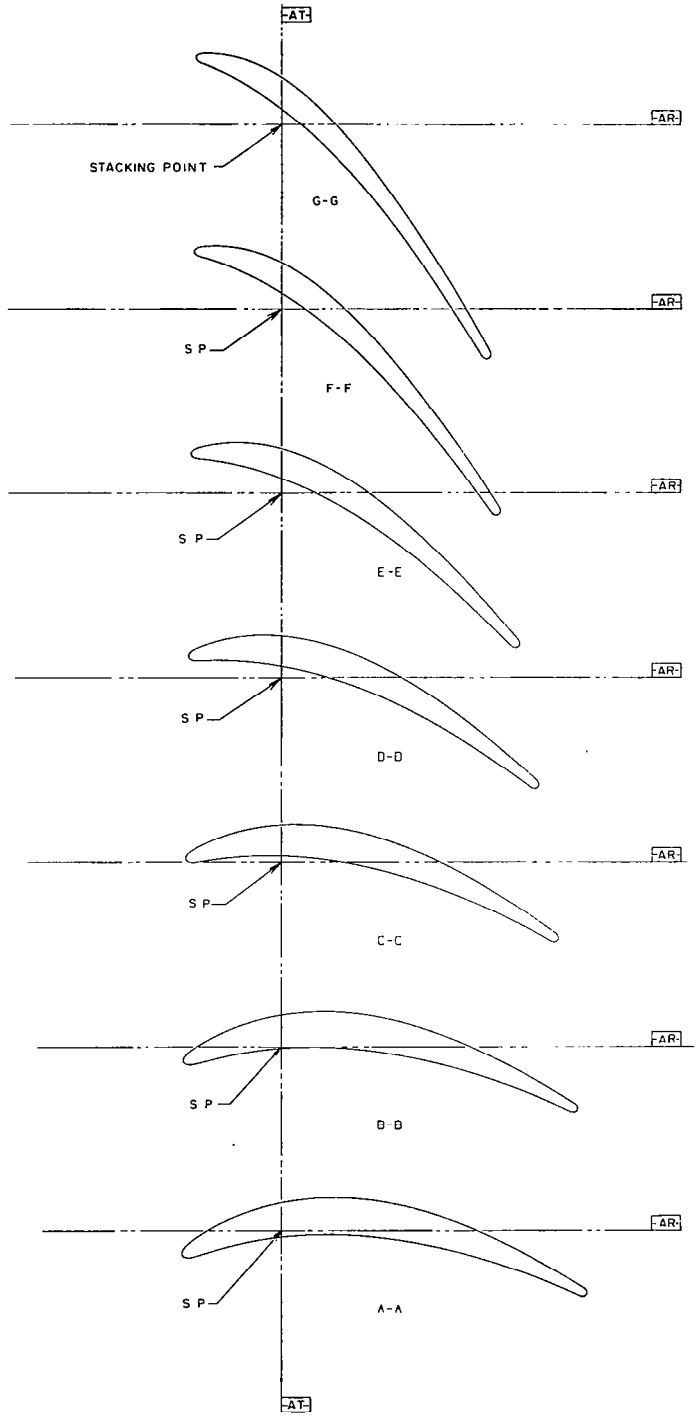


**Figure 27. Stage Three Aft Tandem Blade Precision Master (4012241-972).**

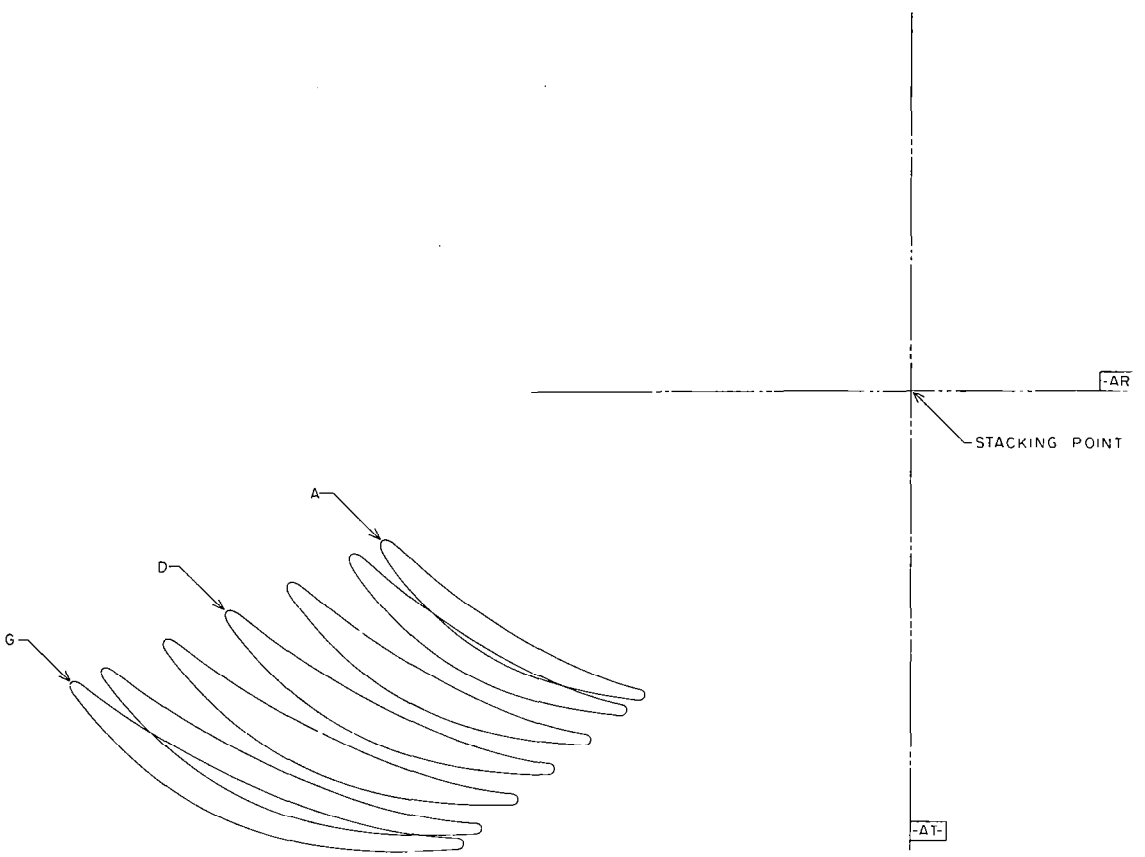


**Figure 28. Stage Two Forward Tandem Vane Stackup (4012241-963).**

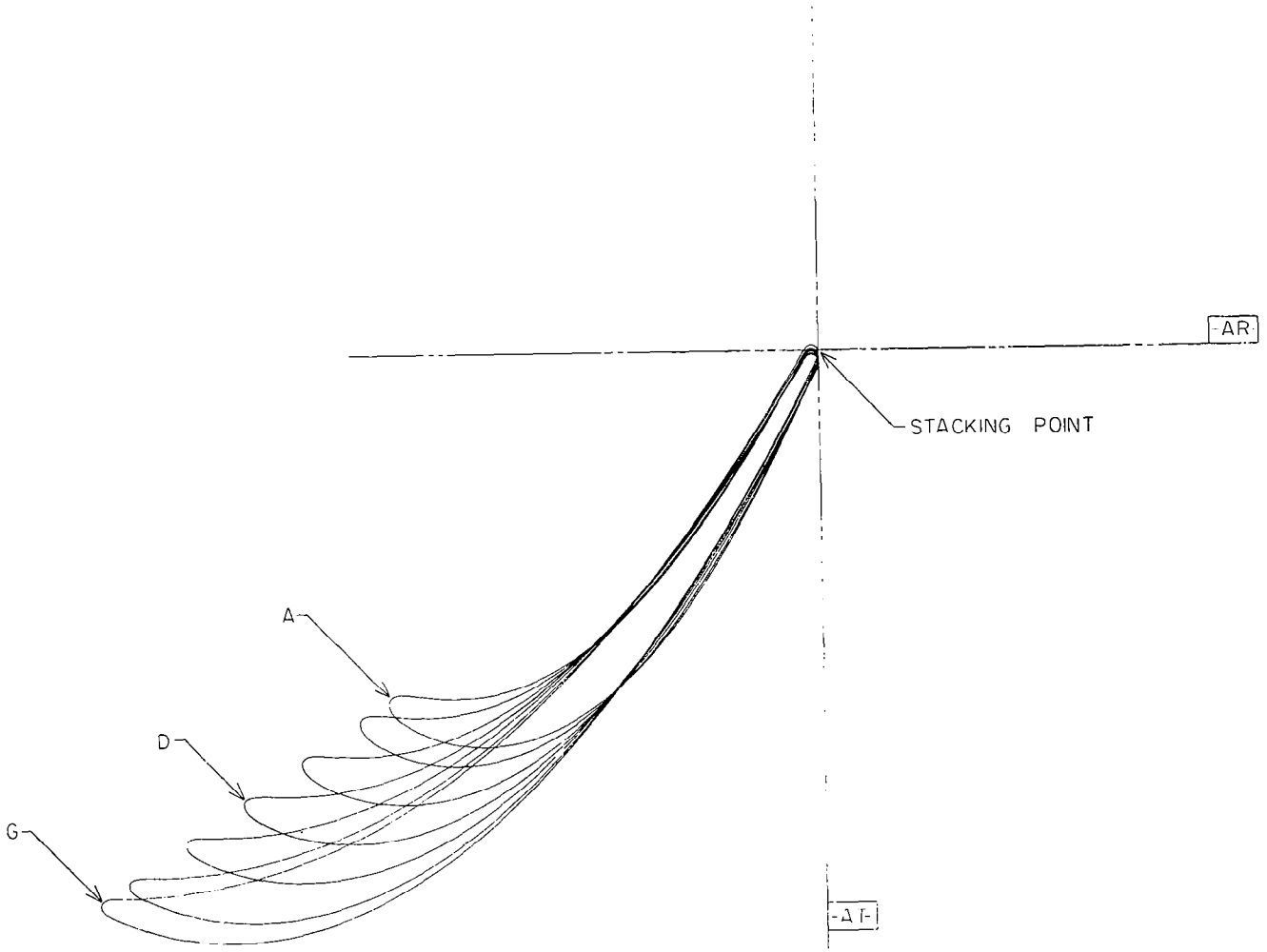


**Figure 29.** Stage Two Aft Tandem Vane Stackup (4012241-965).

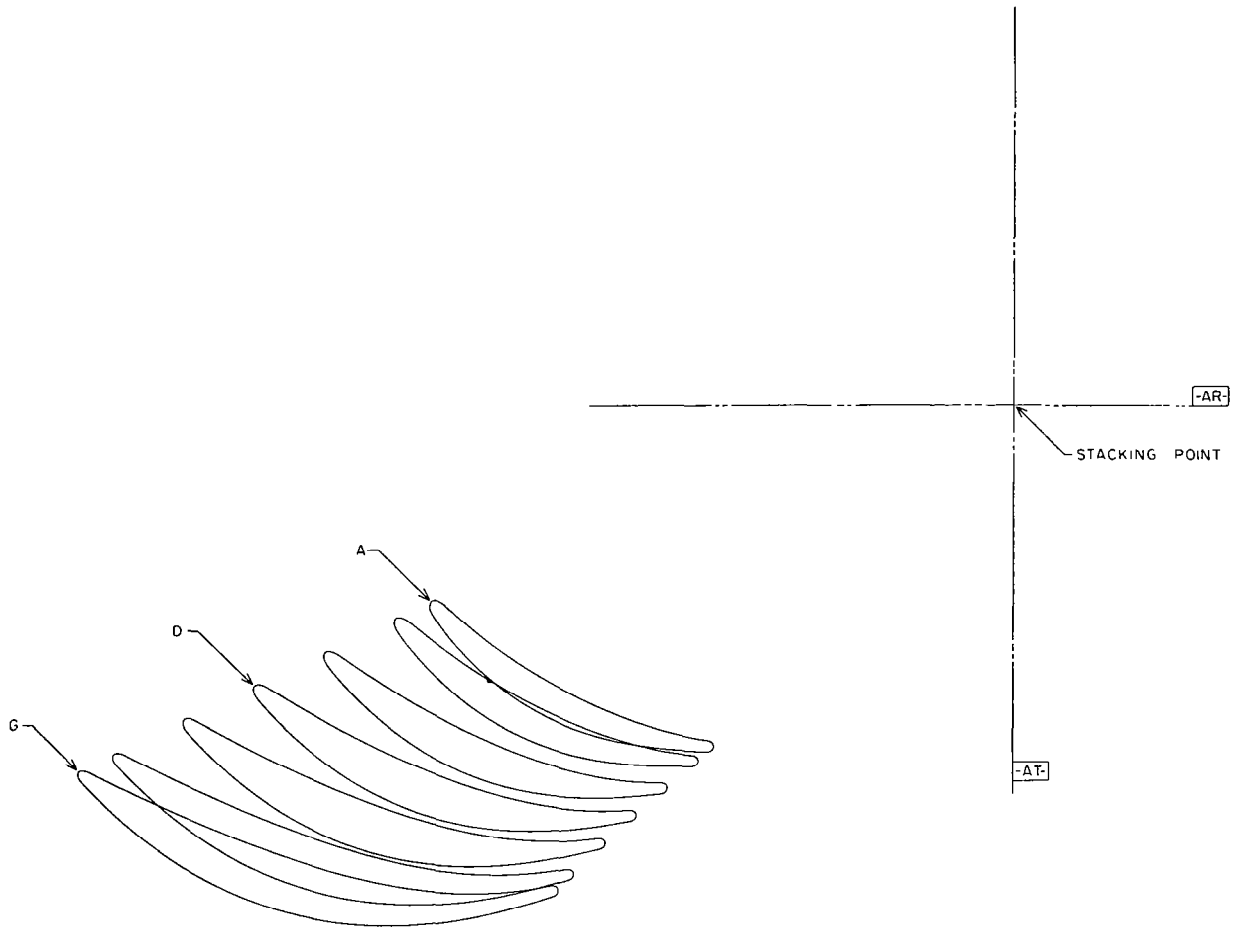


**Figure 30. Stage Three Forward Tandem Vane Stackup (4012241-967).**

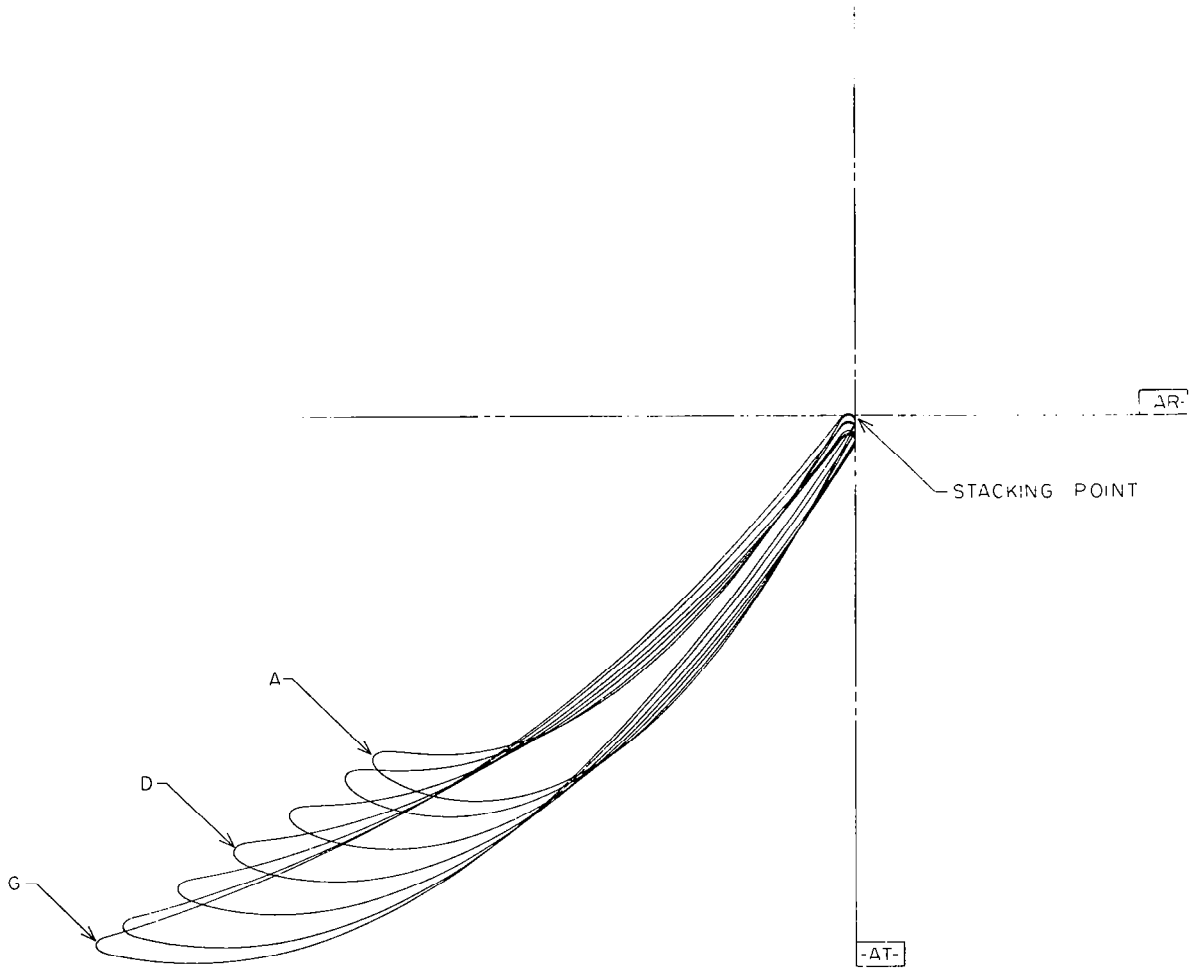


**Figure 31. Stage Three Aft Tandem Vane Stackup (4012241-969).**

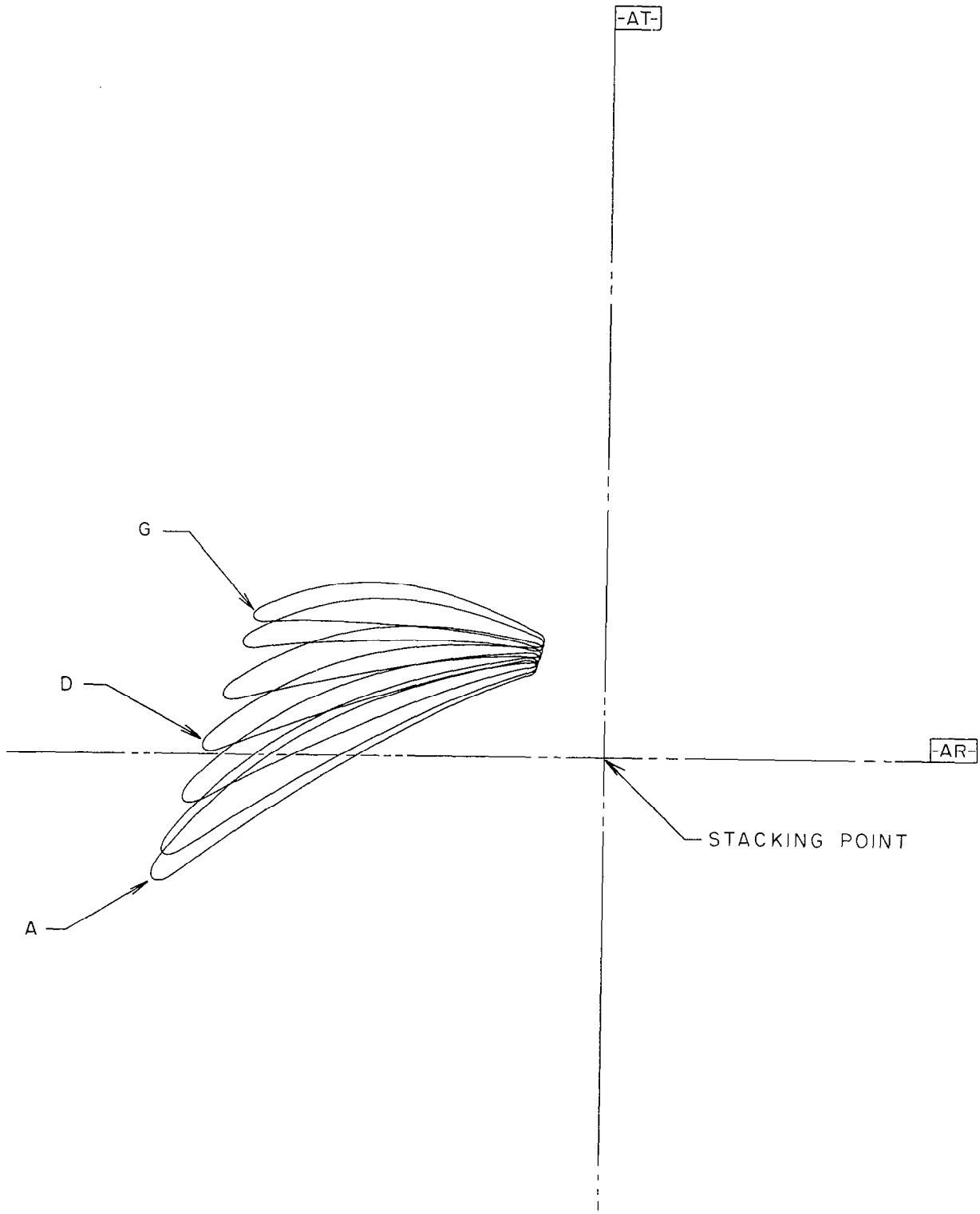


**Figure 32. Stage Three Forward Tandem Blade Stackup (4012241-971).**

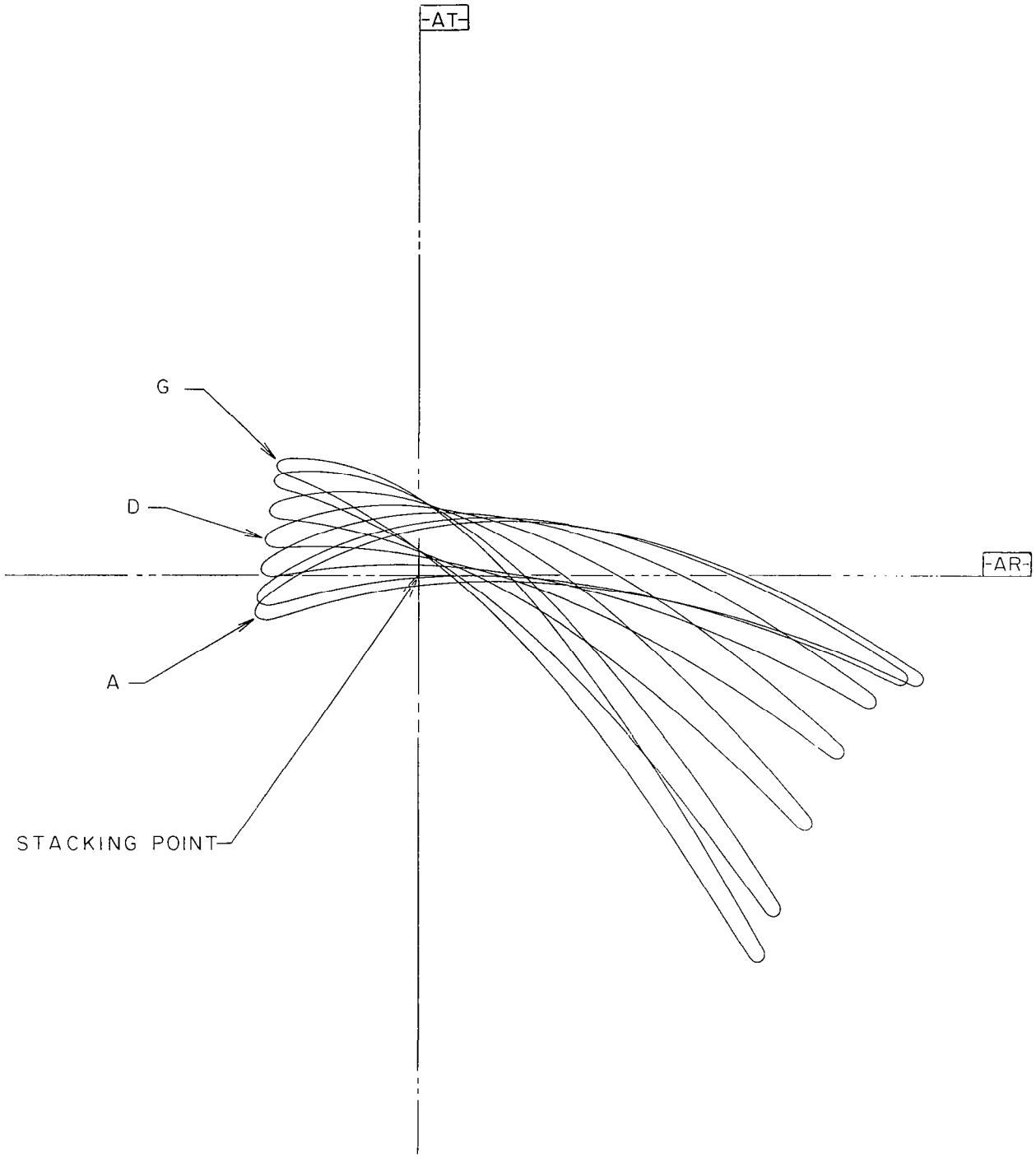


**Figure 33. Stage Three Aft Tandem Blade Stackup (4012241-973).**

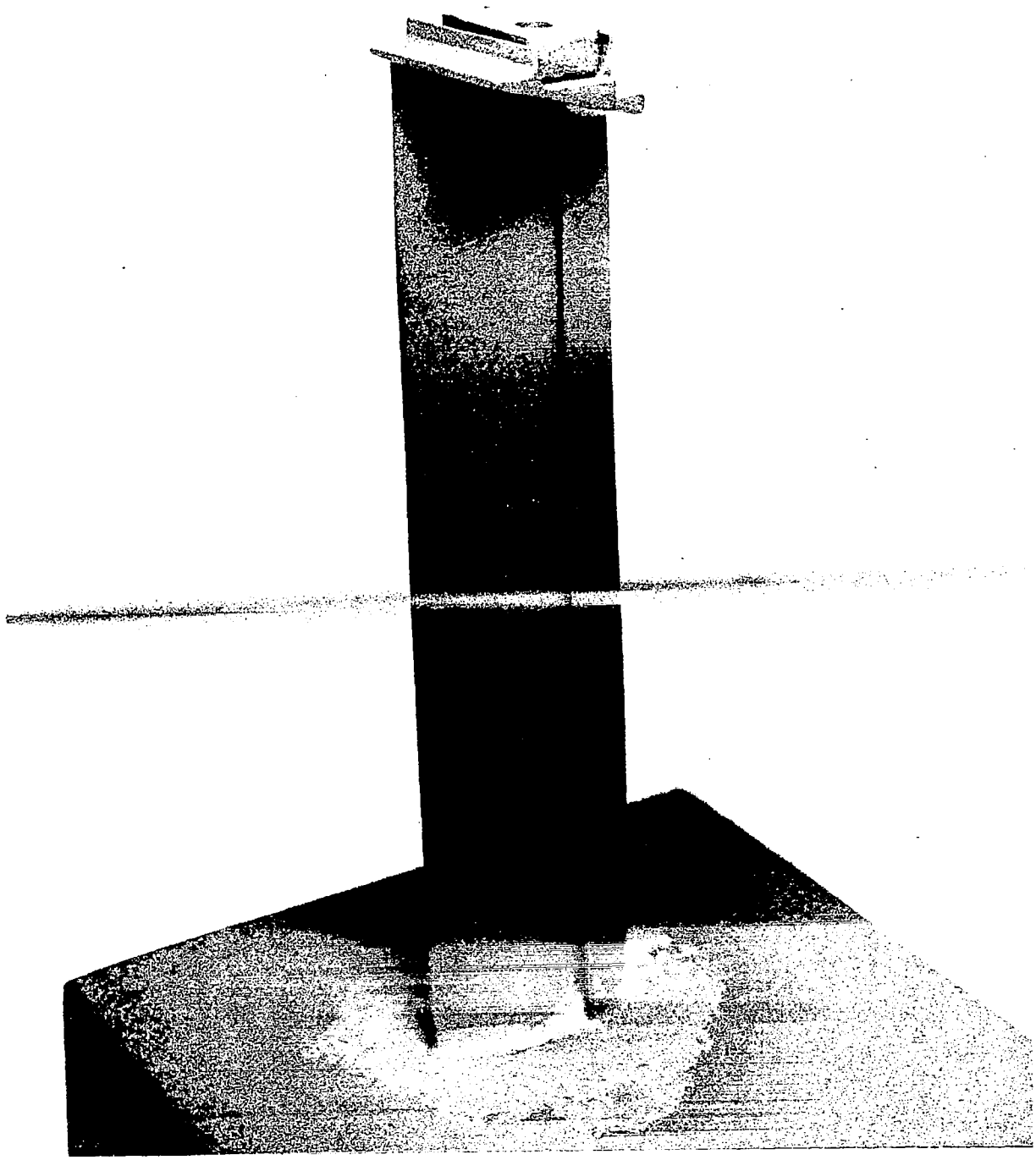

Figure 34. Stage Three Tandem Blade Laboratory Bench Model, Suction Surface.

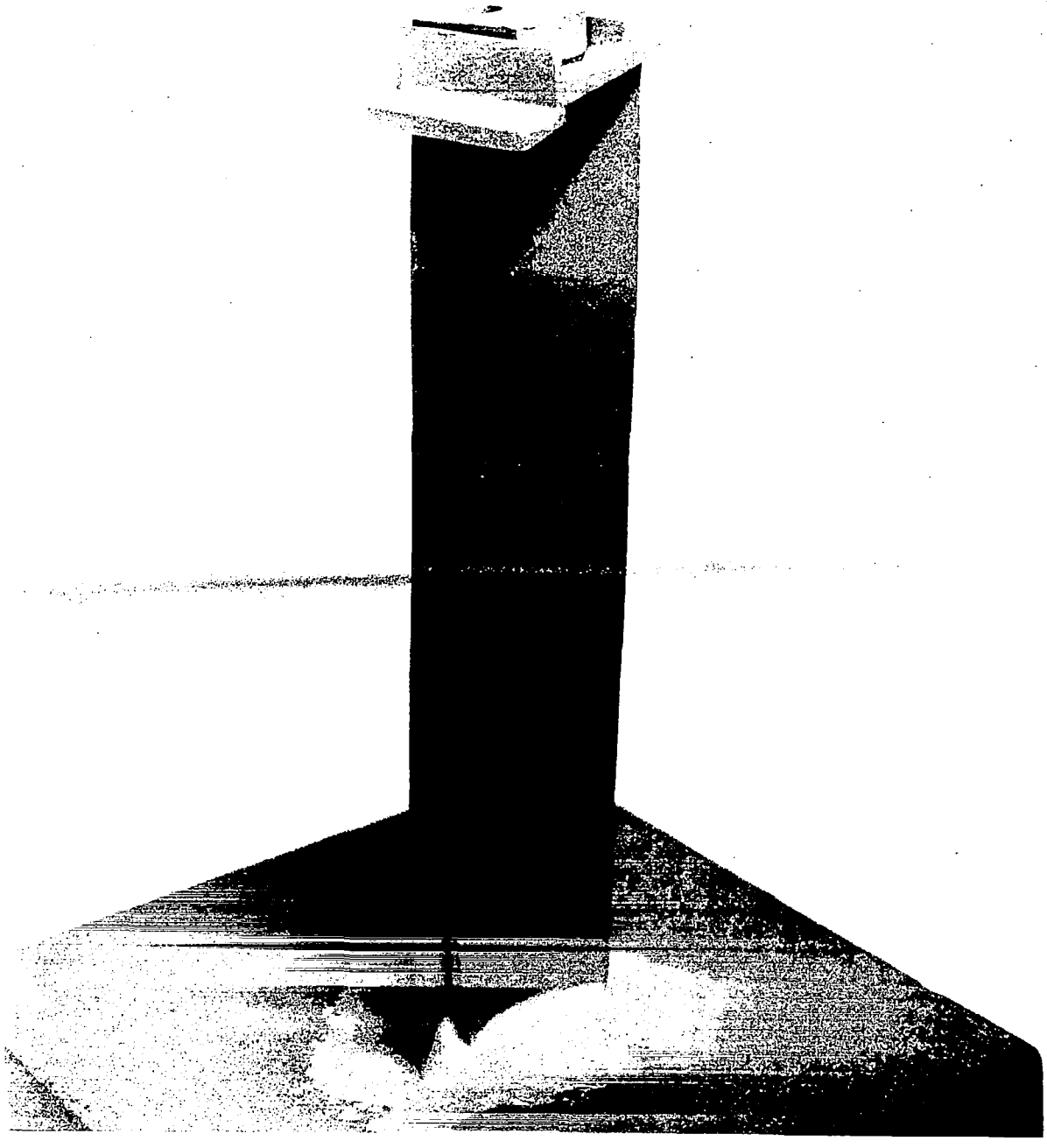

Figure 35. Stage Three Tandem Blade Laboratory Bench Model, Pressure Surface.

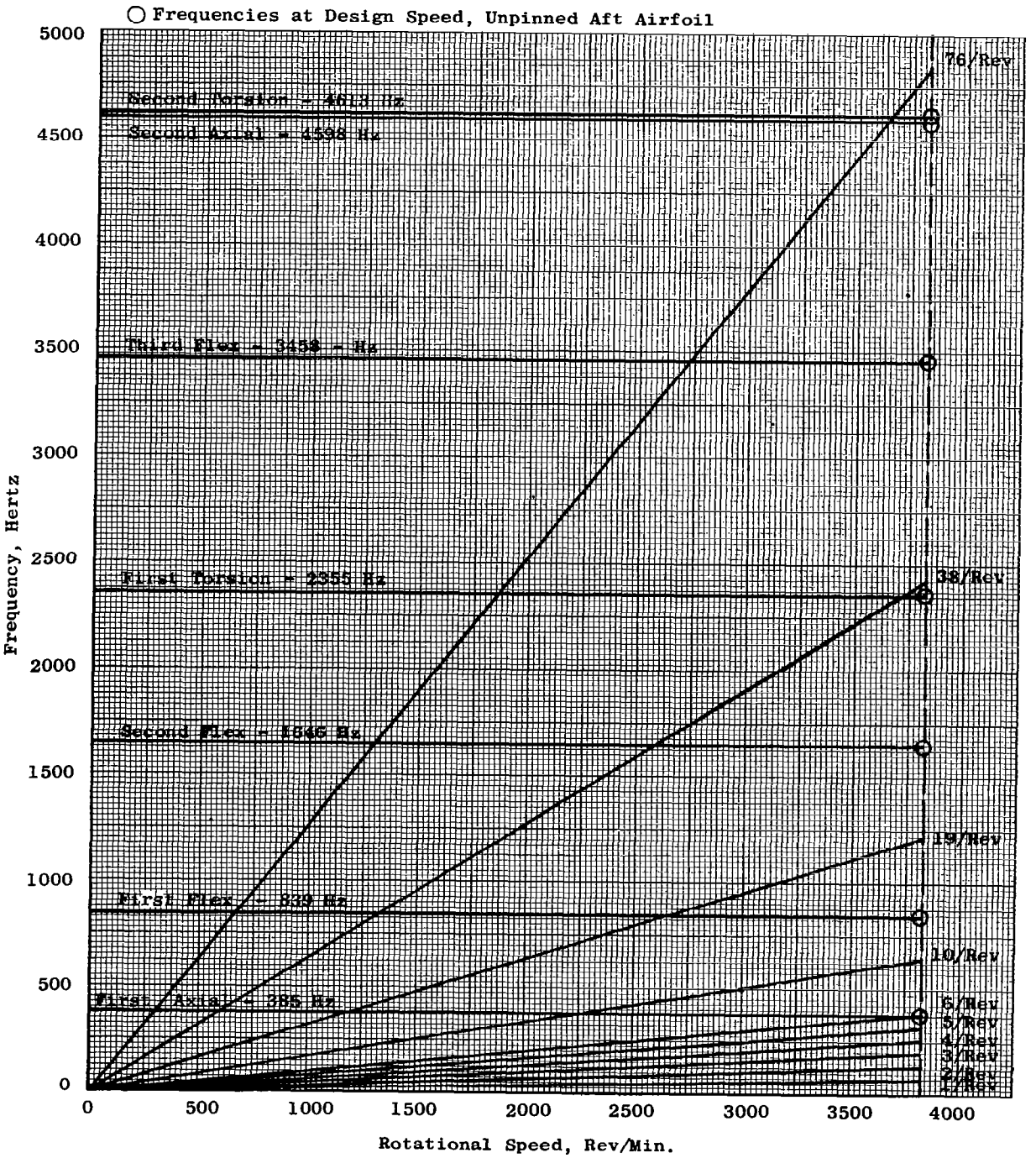


Figure 36. Most Probable Frequencies of Vibration, Stage Three Tandem Blade Aft Airfoil.

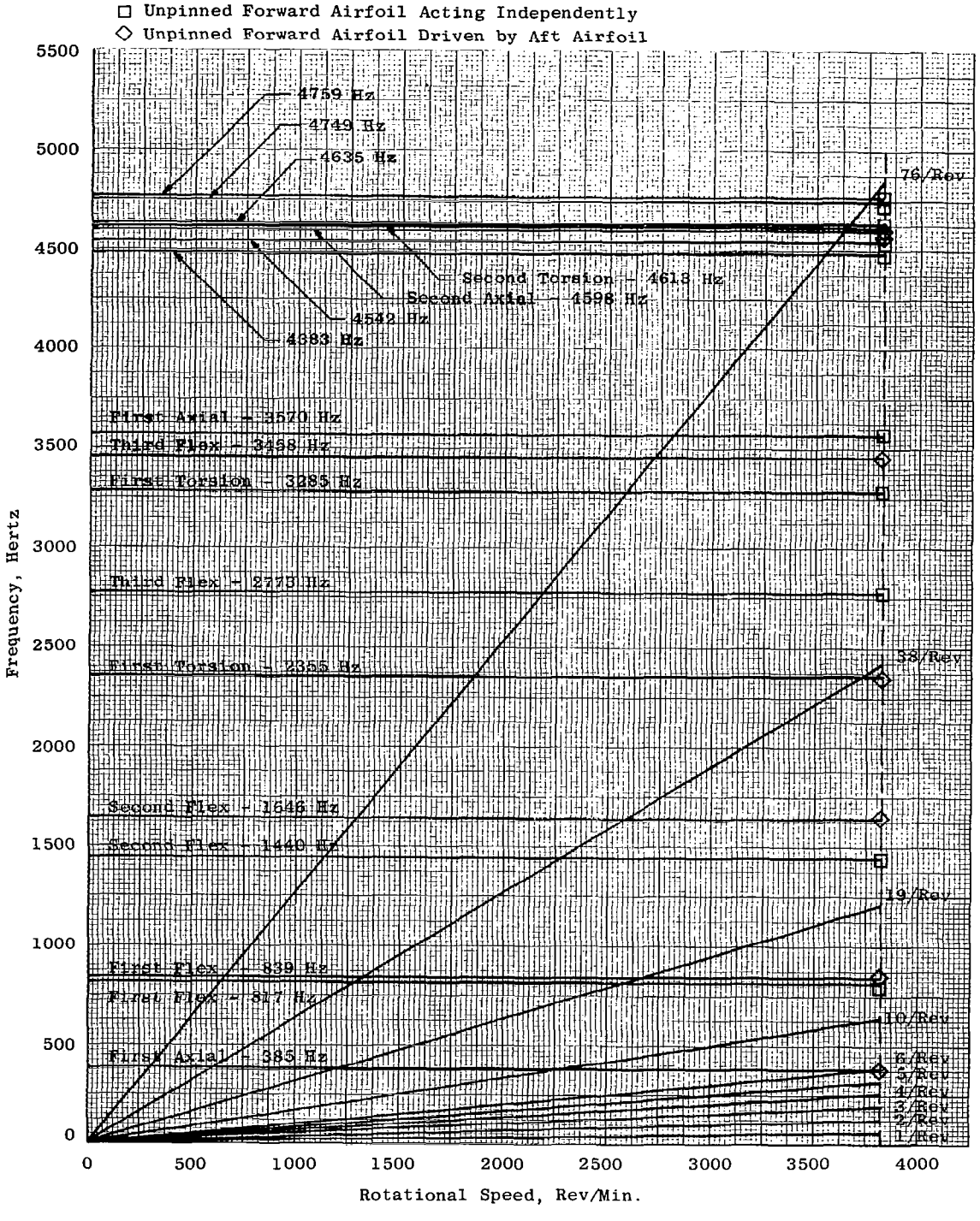


Figure 37. Most Probable Frequencies of Vibration, Stage Three Tandem Blade Forward Airfoil.

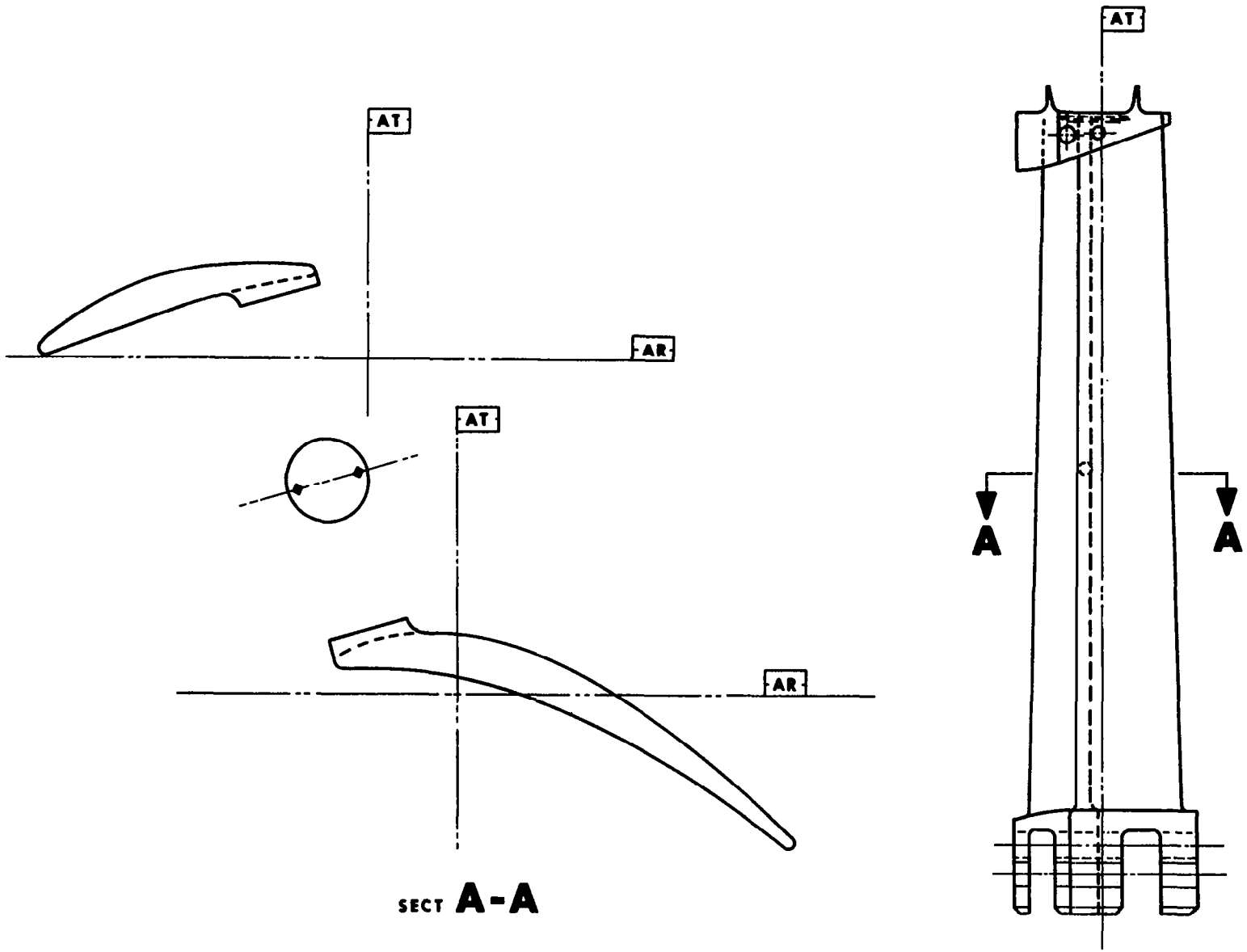


Figure 38. Stage Three Tandem Blade Pinned Configuration.

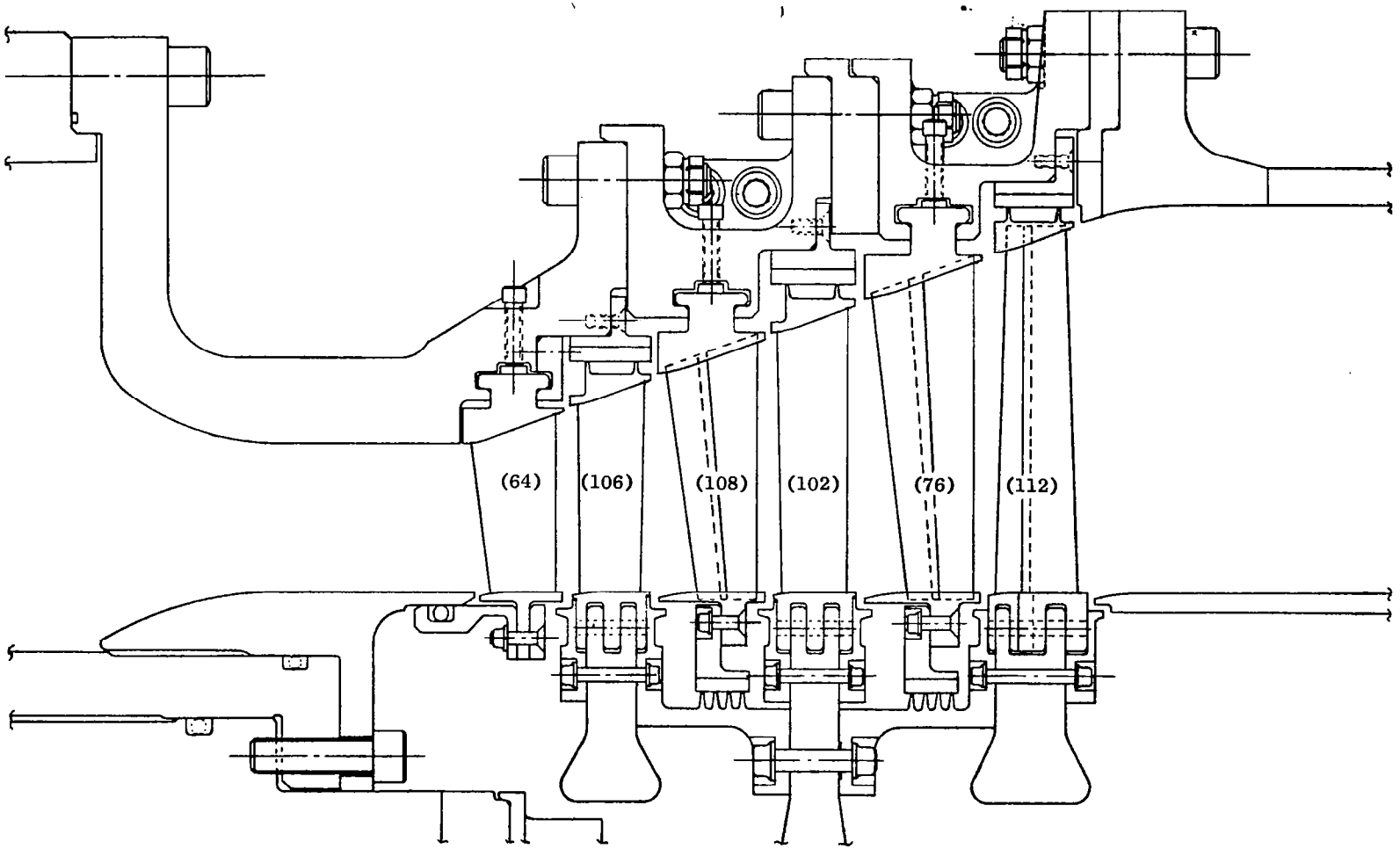


Figure 39. Mechanical Design Flowpath.